CHAPTER 5

Synthesis of chitosan coated manganese dioxide nanoparticles (CMNPs) and its application in the removal of Cr (VI), Cd (II) and Pb (II) from wastewater

Chapter 5: Synthesis of chitosan coated manganese dioxide nanoparticles (CMNPs) and its application in the removal of Cr (VI), Cd (II) and Pb (II) from wastewater

5.1 Introduction

Cr (VI), Cd (II) and Pb (II) are widely spread into the environment and has carcinogenic properties. Chromium (VI) contamination mainly originates from leather tanning unit, steel production, electroplating and textile processing units [Bashir et al., 2020]. The major causes of Cd (II) contamination in the environment include several industrial activities, pesticides used in the agriculture, disposal of cigarette, paint waste and disposal of Cd/Ni batteries [Rao et al., 2010]. Pb (II) is a highly toxic heavy metal, which enters into the environment through several industrial units like battery industries, metal plating, ceramic, glass manufacturing unit [Goel et al., 2005; Momcilovic et al., 2011].

Various technologies such as precipitation, cementation, coagulation and flocculation, solvent extraction, osmosis, reverse osmosis, electrodialysis and ion exchange have been widely used for the removal of Cr (VI), Cd (II) and Pb (II) from the industrial effluent, municipal waste and drinking water [Li et al., 2020a; Renu et al., 2017]. Most of the above-mentioned technologies are very expensive at industrial scale and engender secondary chemical sludge [Fang et al., 2019]. In addition, none of these technologies are capable of reducing Cr (VI) to any other less fatal form [Jin et al., 2017]. Biosorption has been considered as an inexpensive and highly effective method for the removal of toxic heavy metal ions from liquid phase [Jobby et al., 2018]. A large number of biomaterials such as activated carbon, lignite, bentonite and nanoparticles have been utilized as adsorbents for heavy metal ions [Gadd, 2008]. Nowadays, application of nanoparticles in heavy metal adsorption are of contemporary interest [Zhang et al., 2020b]. Nanoparticles also have applications in medical science, fabrications of electronic devices and energy production [Kumar et al., 2015]. The large surface area of small sized nanoparticle is considered as suitable adsorbent property for the removal of heavy metal ions such as Cr (VI), Cd (II) and Pb (II). Nanoparticles are synthesized through several conventional methods such as chemical precipitation, photochemical reduction and solvent extraction etc [Abdelgawad et al., 2017; Souri et al., 2019]. Compared to above mentioned conventional methods, green synthesis of nanoparticles by using plant extract is considered as better option due to its eco-friendly nature [Gnanasangeetha and Saralathambavani, 2013].

Chitosan is a biopolymer has large number of functional groups such as hydroxyl, carboxyl and amino which play an important role in the adsorption of heavy metal ions [Youssef et al., 2018; Kaveeshwar et al. 2018].

The present investigation aimed at the design and development of chitosan-coated MnO_2 nanoparticles (CMNPs) by green route using *Citrus limetta* peel extract for the removal of Cr (VI), Cd (II) and Pb (II) from liquid phase. Chitosan enhances surface area and functional groups on the surface of MnO_2 nanoparticles. Further, synthesized nanoparticles were characterized using FE-SEM, HR-TEM, EDX, elemental mapping, XPS, BET, DLS, FTIR. The ANN modeling has been performed to compare experimental and predicted values. Dimensionless numbers and diffusivity coefficients have been used to delineate the molecular dynamics in adsorption [Biswas et al., 2005] which are also imperative for designing and scaling-up continuous reactors [Chong and Hernandez, 2018; Hua et al., 2018].

5.2.0 Characterization of CMNPs

5.2.1 FTIR analysis

FTIR spectrum of Chitosan, MNPs, CMNPs and heavy metal ions loaded CMNPs is shown in Figure 5.1.

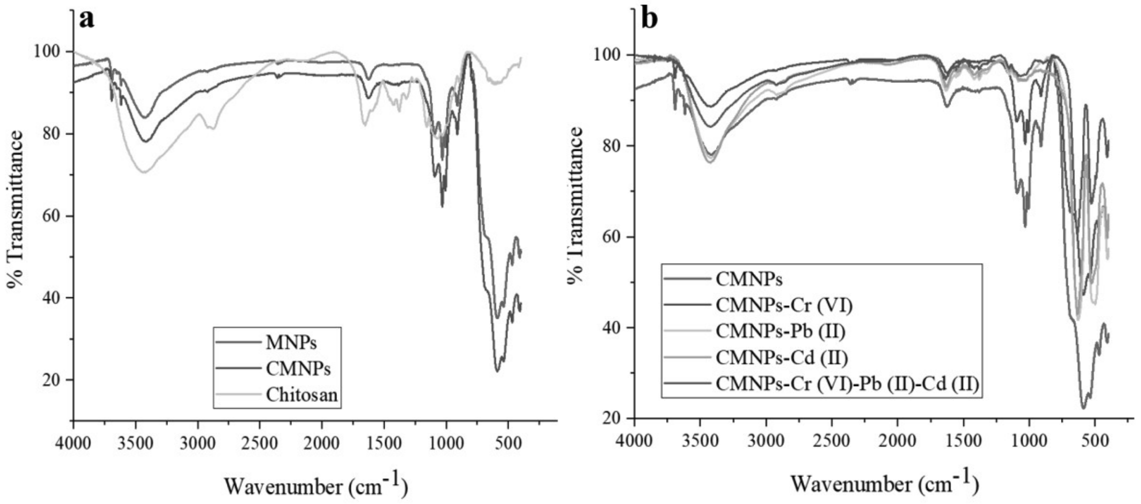

Figure 5.1 FTIR spectra of chitosan, MNPs, CMNPs **(a)** and heavy metal loaded CMNPs **(b)**

The broad bands between the range of 3000 to 3800 cm^{-1} indicated O-H and N-H stretching of H-bonded alcohols, phenols and proteins (Figure 5.1 a and b) [Suresh et al., 2016]. The peak at 1500 to 1700 cm^{-1} represented C≡C stretching in the aromatic rings [Tian et al., 2018]. The peaks from 1320 to 1350 cm^{-1} indicated the presence of N-O symmetric stretch of nitrogen containing groups of chitosan (Figure 5.1 a) [Quintelas et al., 2013]. Peaks at 1147.48 cm^{-1} showed the presence of C-O stretch in the ethers and lactones. Peaks at 900 to 1100 cm^{-1} demarcated C-O stretch of alcoholic groups [Fang and Achal, 2018; Jin et al., 2017]. Variations in the FTIR spectra were reported in chitosan, MNPs, CMNPs. FTIR depicted the existence of $-NH_2$, -OH, C≡C and C-O on the surface of chitosan, MNPs and CMNPs due to the involvement of organic substance used in the synthesis of nanoparticle. The band pattern of FTIR were also changed after biosorption of heavy metal ions (Figure 5.1 b). The changes in the FTIR spectra were reported at 900-1300 cm^{-1} in the CMNPs loaded with Cr (VI), Cd (II) and Pb (II) in single and ternary metal ion system. The change in the FTIR spectra indicated that C-O and $–NH_2$ groups of chitosan actively participated in the biosorption of Cr (VI), Cd (II) and Pb (II). The maximum variations in the FTIR spectra were reported in the Cd (II), Pb (II) of single and ternary metal ion system and very slight variations were reported in the Cr (VI) loaded CMNPs (Figure 5.1 b). Saha et al., 2013 reported that $–NH_2$ and C-O groups actively participated in the adsorption of heavy metal ions. Samrot et al., 2018 performed the biosorption experiment on chitosan coated iron nanoparticles and reported similar kind of results. Al-Naamani et al., 2018 also performed FTIR analysis of chitosan-ZnO nanocomposites and reported analogous outcome.

5.2.2 HR-TEM

Size and morphology of CMNPs observed by HR-TEM is shown in Figure 5.2.

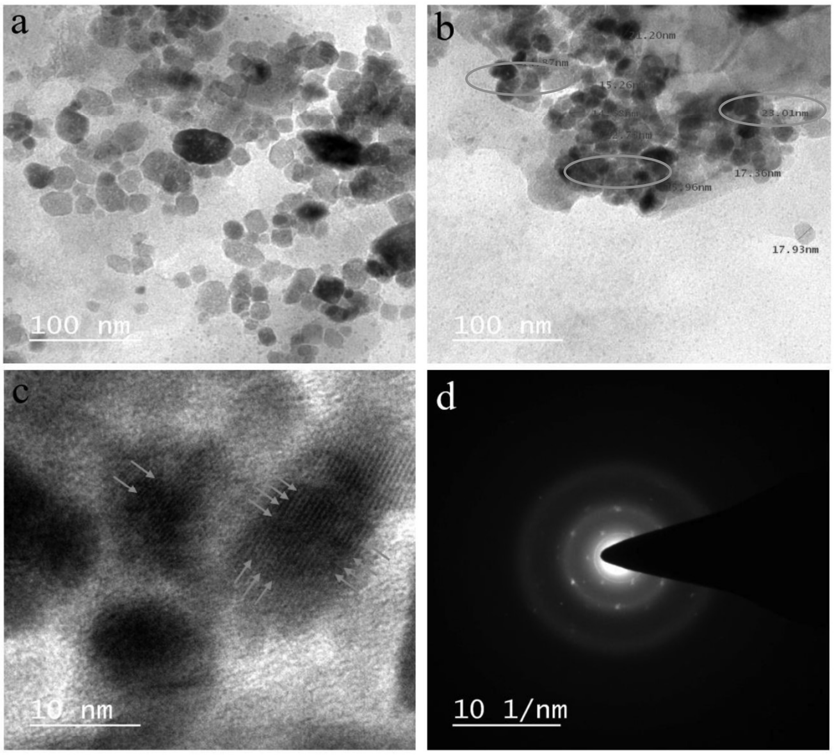

Figure 5.2 Size and shape of CMNPs (a-b), lattice fringes indicated by arrows (c) and SAED pattern of CMNPs (d)

TEM images (Figure 5.2 a-c) showed that the CMNPs were spherical in shape and uniform in size distribution. The average size of nanoparticles was around 14 - 23 nm. The parallel lattice fringes were clearly apparent (Figure 5.2 c) in CMNPs. A crystal lattice is described as arrangement of particles that form a crystal. The spacing observed in the lattice fringes confirmed the crystallinity and structural uniformity in the CMNPs [Ye et al., 2006]. The bright spots in the selected area of SAED pattern showed a diffraction ring which confirmed the crystallinity in CMNPs (Figure 5.2 d) [Cheng and Walker, 2010]. Presence of crystallinity in CMNPs provided option for performing multiple adsorption-desorption cycles without significant degradation. The small size and spherical shape of CMNPs provided large specific surface area for the binding of heavy metal ions. Unsoy et al., 2012 synthesized and characterized chitosan-coated iron oxide nanoparticles and reported crystalline structure. Authors also observed similar types of lattice fringes in TEM images. Guo et al., 2014 synthesized MnO2 microsphere assembled from nanofilms. Authors characterized synthesized materials using TEM analysis and reported similar observations.

5.2.3 HR-SEM

The size and surface morphology of CMNPs were characterized through HR-SEM. The surface properties of biosorbent such as size, surface area, surface roughness or smoothness play an important role in biosorption of heavy metals [Guo et al., 2014; Buccolieri et al., 2017]. The HR-SEM images of CMNPs is shown in Figure 5.3.

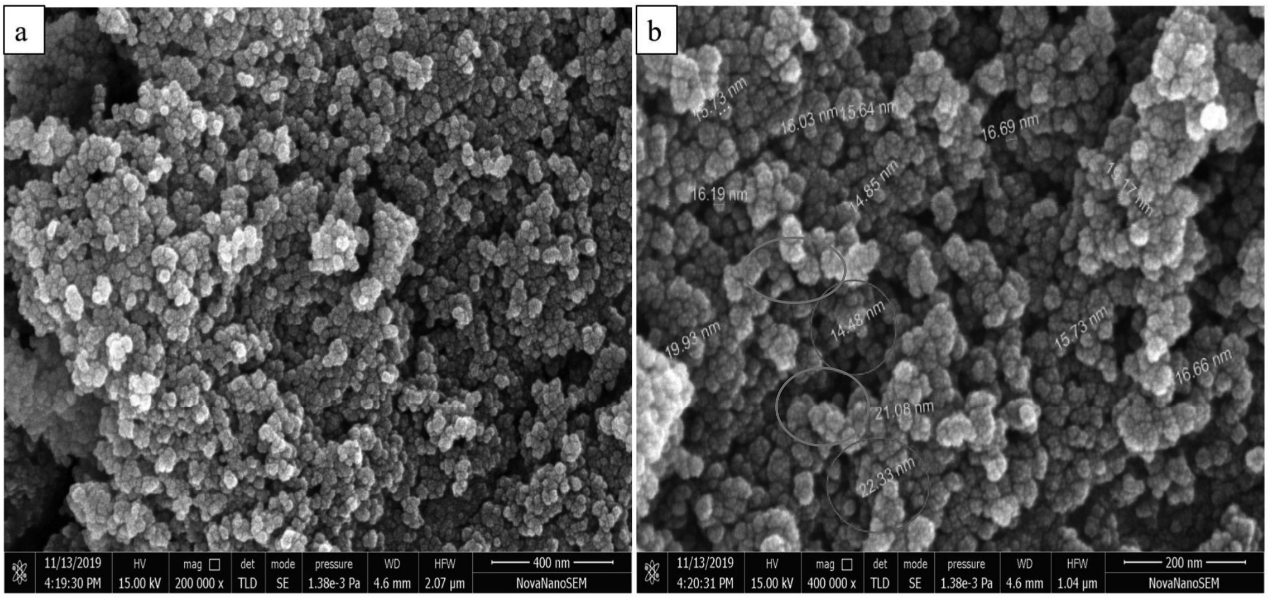

Figure 5.3 HR-SEM micrographs of CMNPs **(a, b)**

It became evident from Figure 5.3 a and b that CMNPs were uniformly aggregated and spherical in shape. The average size of CMNPs was observed in the range of 14 - 22 nm. Almost similar range of CMNPs size was also observed in the TEM images (Figure 5.2b). The SEM images also showed the rough surface morphology of CMNPs. The rough surface and small size of CMNPs delineates preferential biosorption property for the removal of heavy metals. The rough surface and small size of CMNPs delineates preferential biosorption property for the removal of heavy metals. The rough surface and small size of CMNPs might have provided enhanced surface area which supported the biosorption of Cr (VI), Cd and Pb from liquid phase [Xu et al., 2011; Sarma et al., 2019]. Chitosan coating rendered surface of nanoparticles porous and uneven morphologically [Liu et al., 2012; Hu et al., 2016].

5.2.4 EDX Analysis and Elemental mapping

The EDX analysis was performed to confirm the presence of elements which remained bound after biosorption such as Cr (VI), Cd (II) and Pb (II) and the element which played a major role in the synthesis of CMNPs was also confirmed. EDX analysis of CMNPs before and after heavy metal biosorption is shown in the Figure 5.4.

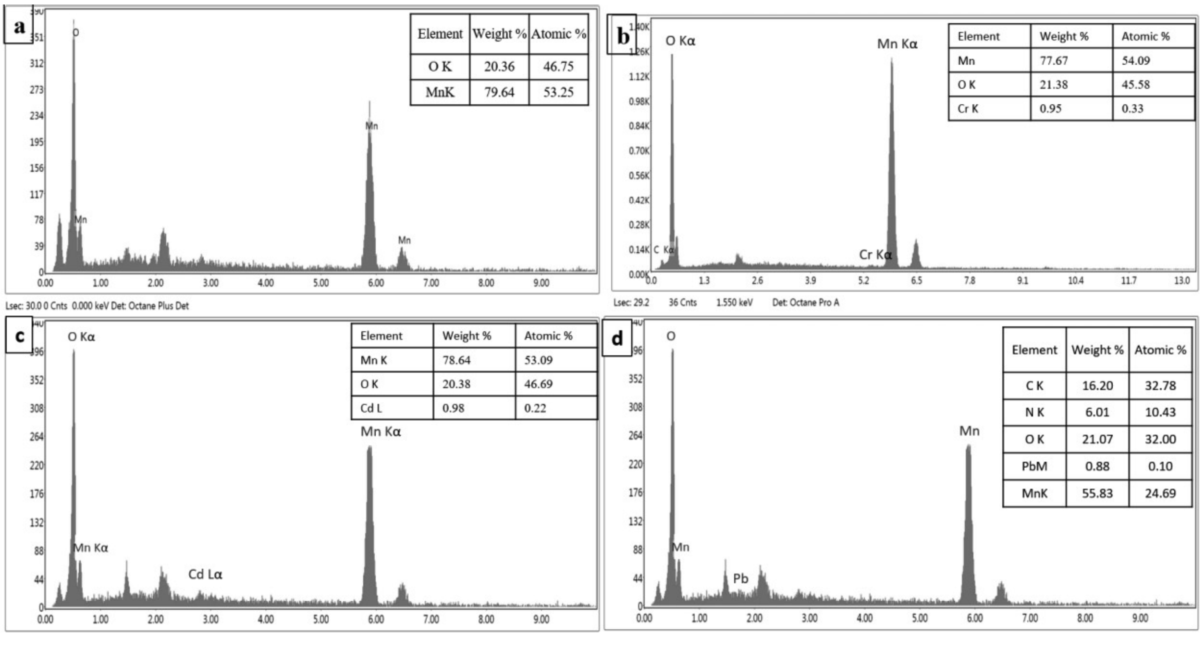

a

Element	Weight %	Atomic %
O K	20.36	46.75
MnK	79.64	53.25

b

Element	Weight %	Atomic %
Mn	77.67	54.09
O K	21.38	45.58
Cr K	0.95	0.33

c

Element	Weight %	Atomic %
Mn K	78.64	53.09
O K	20.38	46.69
Cd L	0.98	0.22

d

Element	Weight %	Atomic %
C K	16.20	32.78
N K	6.01	10.43
O K	21.07	32.00
PbM	0.88	0.10
MnK	55.83	24.69

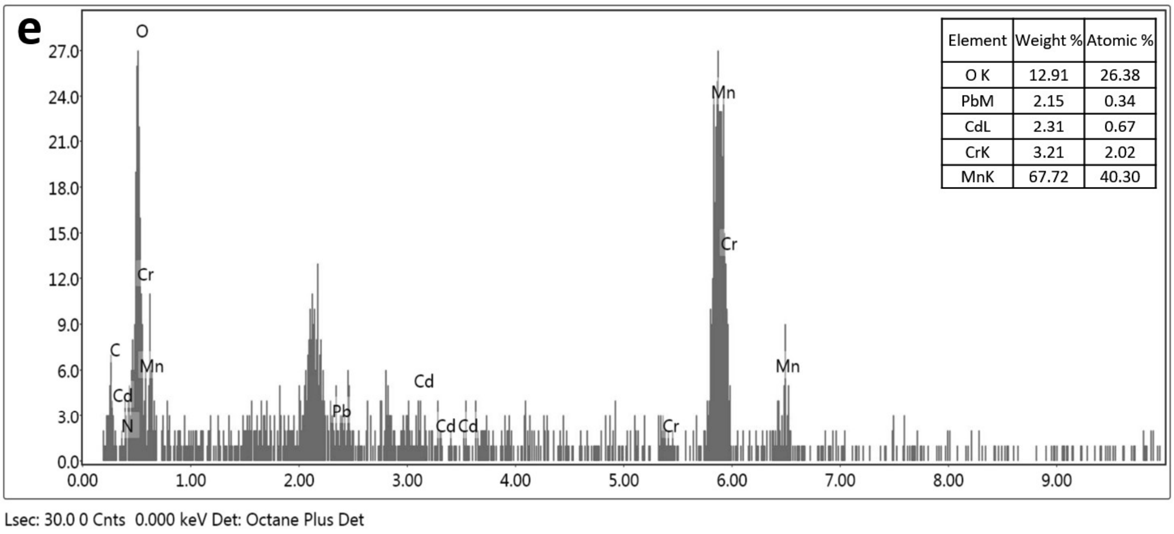

Figure 5.4 EDX analysis of CMNPs before **(a)** and after Cr (VI) **(b),** Cd (II) **(c),** Pb (II) **(d)** and ternary **(e)** metal ion biosorption

Elemental analysis (Figure 5.4a) illustrated that manganese and oxygen were major elements in the CMNPs, which in turn reflected the efficacious synthesis of MnO_2 nanoparticle [Jaganyi et al., 2013; Cherian et al., 2016]. Other minor peaks of carbon were attributed to chitosan coating on MnO_2 nanoparticles. The EDX analysis of CMNPs after heavy metal biosorption confirmed the presence of Cr (VI) (Figure 5.4 b), Cd (II) (Figure 5.4 c) and Pb (II) (Figure 5.4 d) on the CMNPs surface in single metal ion system. Figure 5.4e confirmed the biosorption of all three metal ion on CMNPs surface in the ternary metal ion system. Tho et al., 2021 investigated the adsorption of As (III), Cd (II), Pb (II) and Cr (VI) by ZnO nanoparticle modified biochar derived from cassava root husk modified and reported the presence of As (III), Cd (II), Pb (II) and Cr (VI) on the surface of adsorbent in EDX. Muhammad et al., 2020 performed Cr (VI) and Ni (II) biosorption on polyaniline, iron oxide and their composites. Authors also did EDX to confirm the elemental compositions of the nanomaterials and reported similar kind of observations.

Elemental Mapping also confirmed the presence of elements on the surface of CMNPs. The elemental mapping of heavy metal ions loaded CMNPs is shown in Figure 5.5.

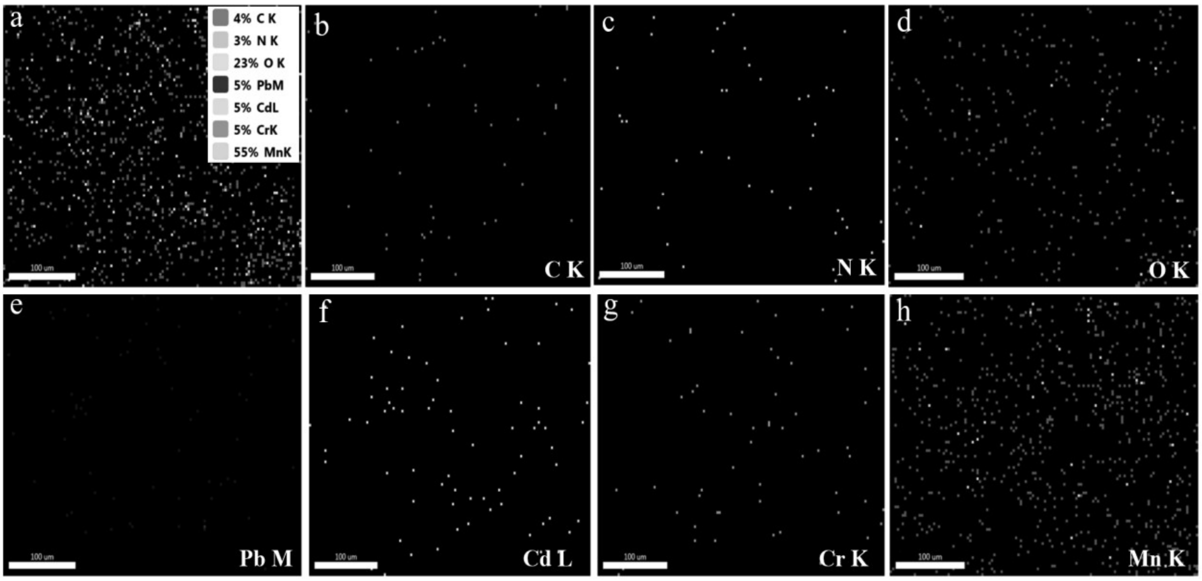

Figure 5.5. Elemental mapping of CMNPs after heavy metal biosorption. Elemental mapping representing distribution of all elements (**a**), carbon (**b**), nitrogen (**c**), oxygen (**d**), Pb (II) (**e**), Cd (II) (**f**), Cr (**g**) and Mn (**h**).

Large amount of Mn (55 %) and O (23 %) were observed in the elemental mapping which are the major component of nanoparticles (Figure 5.5 a, d, h). The presence of C (Figure 5.5 b) and N (Figure 5.5 c) are the component of chitosan and confirmed the chitosan coating on MnO_2 nanoparticles. The homogeneous distribution of Pb (II) (Figure 5.5 e), Cd (II) (Figure 5.5 f) and Cr (VI) (Figure 5.5 g) was also reported in the elemental mapping which confirmed the biosortion of heavy metal ions on the surface of CMNPs. Dinh et al., 2020b performed the SEM elemental mapping of chitosan-MnO_2 nanocomposite and reported similar kind of results. Tho et al., 2021 performed multiple heavy metal (As^{+3}, Pb^{+2}, Cd^{+2} and Cr^{+6}) biosorption using ZnO nanoparticle coated biochar. Authors also investigated elemental mapping and reported biosorption of heavy metal ions on the surface of modified bichar.

5.2.5 CMNPs size measurement using dynamic light scattering (DLS)

DLS has been widely used for the measurement of size of nanoparticles in the liquid phase. The hydrodynamic radius of CMNPs was measured using zeta sizer instrument and graph is shown in Figure 5.6.

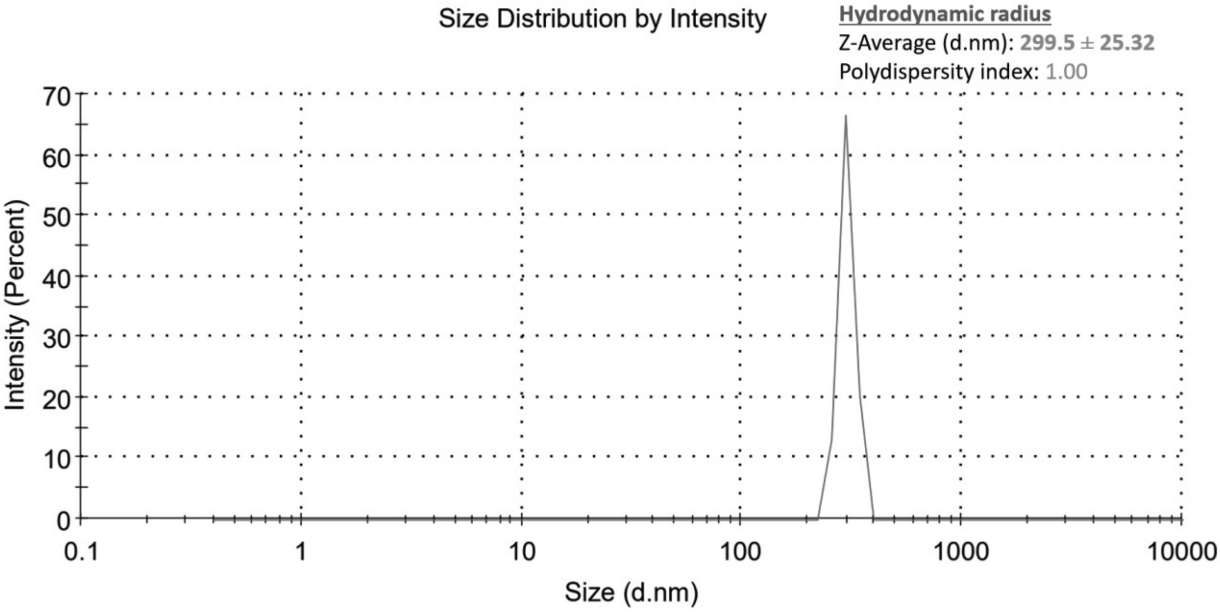

Figure 5.6 DLS analysis of CMNPs

The DLS analysis indicate the average size of CMNPs was 299.5 ± 25.32 nm. The polydispersity index of CMNPs were reported 1.00. Several study have been performed on the size measurement of nanoparticles by DLS [Takechi-Haraya et al., 2018; Bailey-Hytholt et al., 2021]. Sikora et al., 2016 measured size of silica nanoparticles in serum using DLS. Chaturvedi et al., 2020 reported similar results in DLS analysis of trimetallic nanoparticles.

5.2.6 Zero point charge (pH_{zpc})

The coating of chitosan afforded NH_2^+ and H^+ groups on the surface of CMNPs. These groups were the responsible for surface charge [Mondal et al., 2019]. Below pH_{zpc} point, the surface of biosorbent bears positive charge and vice-versa. In the present investigation pH_{ZPC} was recorded as 3.17 (Figure 5.7).

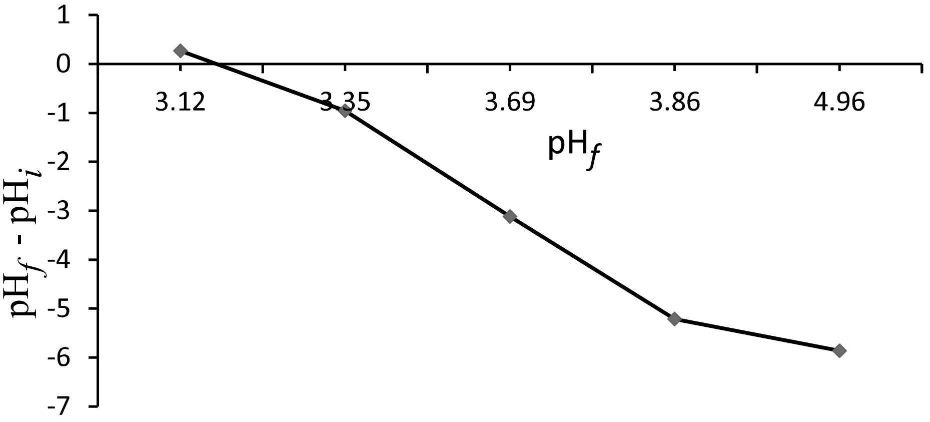

Figure 5.7 pH$_{zpc}$ value of CMNPs

Below the pH 3.17, the surface of CMNPs was positively charged and above this pH (3.17) the surface of CMNPs was negatively charged. Above the pH 3.17, the negative surface of adsorbent was favourable for the biosorption of positively charged heavy metal ions such as Pb^{2+} and Cd^{2+}. Below the pH$_{ZPC}$ value, there was favourable binding of Cr (VI) on the surface of CMNPs. Fato et al., 2019 investigated the multiple metal ion removal from river water using mesoporous magnetite nanoparticle adsorbent. Authors observed the pHzpc of adsorbent as 4.5. The maximum Cr (VI) removal was achieved at pH 2. This was attributed to the fact that Cr (VI) exists as HCrO^{4-} ion at acidic pH [Mondal et al., 2019] and these negatively charged chromate ions were attracted by positively charged (protonated) surface of CMNPs. Miyittah et al., 2016 estimated the pH$_{zpc}$ value of MnO$_2$ nanoparticles as 4.97. Authors estimated these values through acid-base potentiometric titrations. He et al., 2019 investigated pH$_{zpc}$ of imprinted magnetic biosorbent for removal of Pb (II). Authors reported 4.23 pH$_{zpc}$ of biosorbent which indicated that pH > pH$_{zpc}$ (4.23) was suitable for removal of heavy metal ions. Egbosiuba et al., 2021 performed Cr (VI), Ni (II), Fe (II) and Cd (II) adsorption on KIAgNPs decorated MWCNTs nano adsorbent. Authors concluded pH$_{zpc}$ as 6.0 and greater than this is suitable for adsorption of Cd (II) ions.

5.2.7 Specific surface area

In the present work, the specific surface area of CMNPs was recorded as 76.19 (m^2/g). A comparative analysis of specific surface area of CMNPs with other nanoparticles is shown in Table 5.1.

Table 5.1 Specific surface area of CMNPs and other nanoparticles

Nanoparticles	**Specific surface area (m^2/g)**	**References**
CuO nanoparticles	84.32	[Gupta et al., 2016]
Yerba mate extracts coated Fe nanoparticles	17.52	[Garcia et al., 2019]
Green tea extracts coated Fe nanoparticles	1.80	[Garcia et al., 2019]
CuS nano-spheres decorated reduced graphene oxide aerogel composite	191.99	[Bano et al., 2020]
Graphene oxide modified magnetic chitosan nanocomposites	5.40	[Subedi et al., 2019]
Magnetite nanoparticles	31.55	[Ataabadi et al., 2015]
Graphene/silica nano-sheets with polypyrrole-graphene/silica (GS-PPy)	37.60	[Fang et al., 2018]
Fe_3O_4 loaded chitosan nanoparticles	61.48	[Zhang et al., 2019]
Illite/iron nanoparticles	5.53	[Cai et al., 2019]
Modified magnetic chitosan/graphene oxide nanocomposites	132.90	[Hosseinzadeh et al., 2018]
Pd nano-catalyst immobilized on cigarette filter	5.57	[Dorosti et al., 2020]
CMNPs	76.19	[This study]

It became apparent from Table 5.1 that CMNPs have higher specific area as compared to the most of the nanoparticles/ nanocomposites developed in other investigations.

5.2.8 XPS analysis and determination of oxidation state of chromium

The biosorption of Cr (VI), Cd (II) and Pb (II) was confirmed through comparative XPS analysis of CMNPs before and after heavy metal biosorption (Figure 5.8).

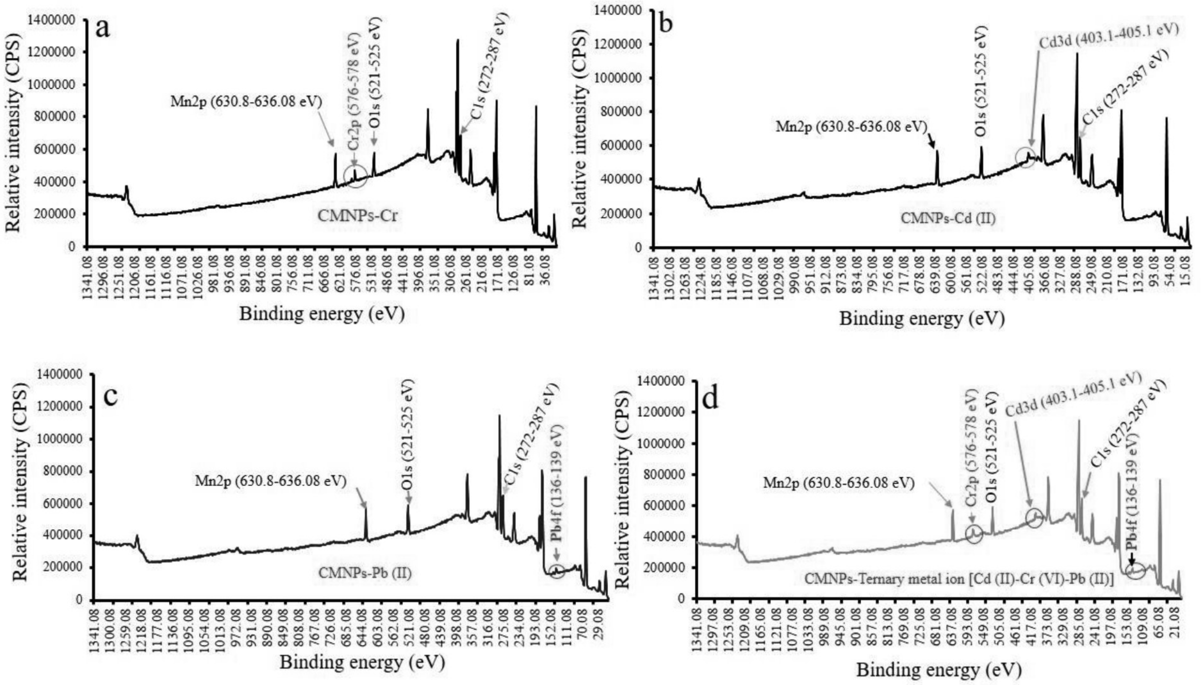

Figure 5.8 XPS of Cr (VI) (**a**), Cd (II) (**b**), Pb (II) (**c**) and ternary metal ion (**d**) biosorption on CMNPs.

The XPS analysis of CMNPs showed manganese at 630.58-636.08 eV, oxygen at 521 - 525 eV and carbon at 272 - 287 eV. The peaks of manganese and oxygen represented the efficacious synthesis of MnO_2 nanoparticle and presence of carbon indicated successful coating of chitosan over MNO_2 nanoparticles. Peaks at 576 - 578 eV in Figure 5.8a indicated biosorption of Cr (VI) on the CMNPs. The chromium loaded CMNPs showed peaks at binding energy 576 - 578 eV which indicated the presence of chromium. Figure 5.8 b and c confirmed the biosorption of Cd (II) and Pb (II) in the energy range of 403.1 to 405.1 eV and 136 to 139 eV respectively. Figure 5.8d indicated the biosorption of Cr (VI), Cd (II) and Pb (II) in the ternary metal ion system. He et al., 2019 investigated Pb (II) adsorption by magnetic imprinted biosorbent and confirmed Pb (II) binding on biosorbent surface through XPS. Meng et al., 2019 did Cd (II) and As (V) adsorption by Ferrihydrite/Manganese dioxide composites. Authors confirmed Cd (II) and As (V) adsorption by XPS analysis. Komarek et al., 2015 explored Cr (VI), Cd (II) and Pb (II) adsorption onto nanomaghetmite. Authors confirmed heavy metal adsorption on nanomaghetmite through XPS analysis.

The reduction of Cr (VI) into Cr (III) was also confirmed through XPS analysis. The amount of Cr (VI) reduced to Cr (III) was estimated through desorption method followed by oxidation ($KMnO_4$). The total amount of Cr (VI) reduced to Cr (III) was calculated as 79.46% of absorbed Chromium. Figure 5.9 shows the incidence of Cr (III) and Cr (VI) on the surface of CMNPs.

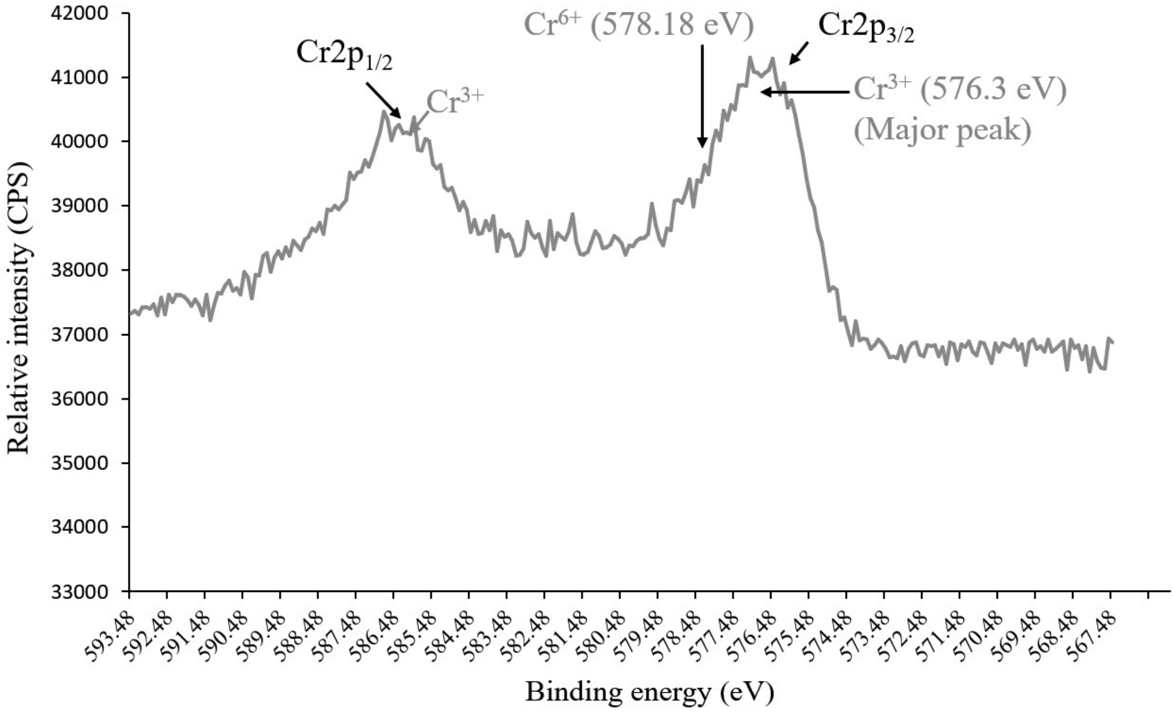

Figure 5.9 Incidence of Cr (III) and Cr (VI) after reduction

High intensity peaks were observed in the range of 576 to 578 eV and 586 to 587 eV (Figure 5.9). These high intensity peaks were attributed to the presence of Cr (III) on CMNPs surface [Guo et al., 2020]. However, no significant peak of Cr (VI) was observed. These results indicated that Cr (VI) on CMNPs reduced to Cr (III) after biosorption. Park et al., 2007 reported high intensity bands of Cr (III) in the range of 577 - 579 eV and 586 - 588 eV, which correspond to Cr2p3/2 and Cr2p1/2 orbital. Sawalha et al., 2007 also reported the reduction of Cr (VI) to Cr (III) on the surface of *Atriplex canescencs*.

5.3.0 Biosorption study

5.3.1 Optimization of process parameters

The effect of pH, temperature, initial metal ion concentration, CMNPs dosage, contact time and agitation on the Cr (VI), Pb (II) and Cd (II) removal was observed. The effect of parameters on Cr (VI), Pb (II) and Cd (II) removal is shown in Figure 5.10, 5.11 and 5.12, respectively

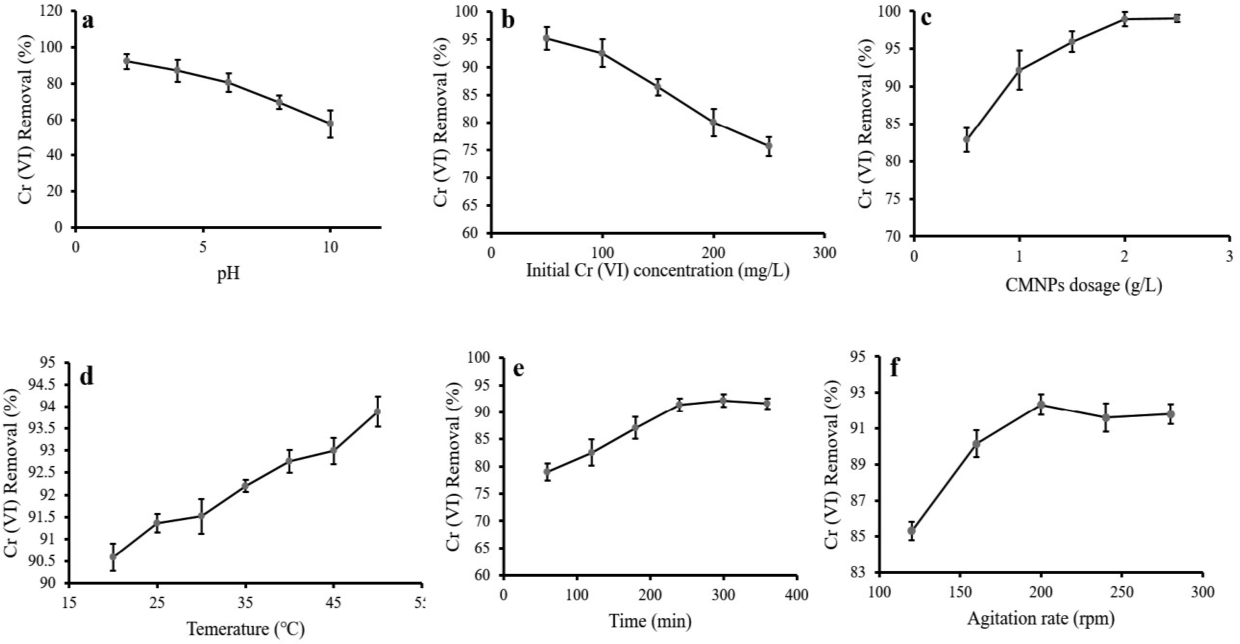

Figure 5.10 Effect of pH (a), initial Cr (VI) concentration (b), CMNPs dosage (c), temperature (d), contact time (e), and agitation rate (f) on Cr (VI) removal using CMNPs

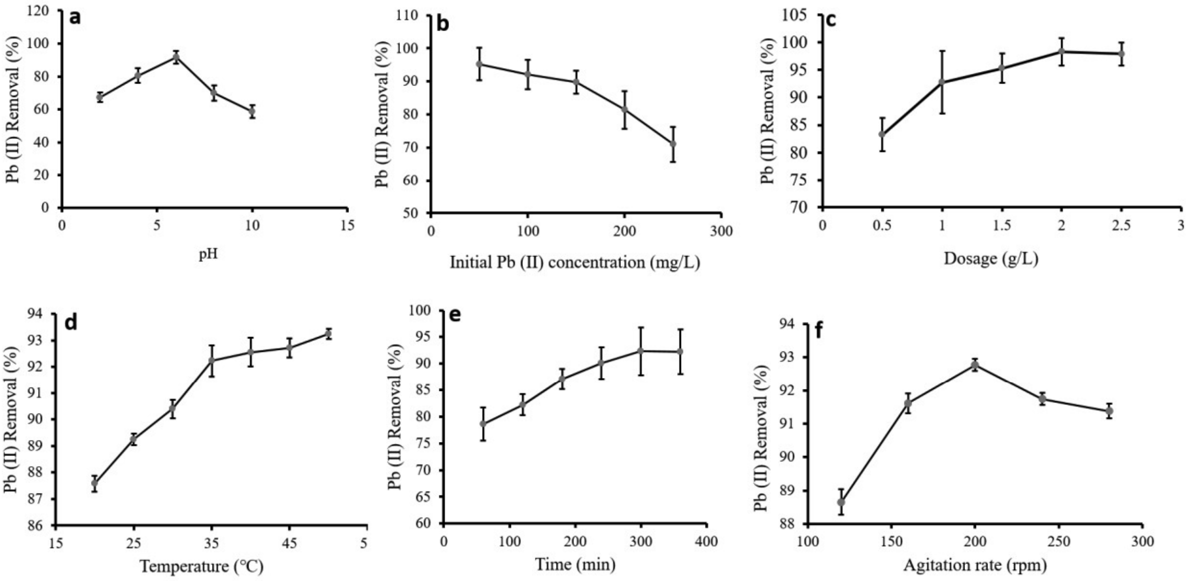

Figure 5.11 Effect of pH (a), initial Pb (II) concentration (b), CMNPs dosage (c), temperature (d), contact time (e) and agitation rate (f) for Pb (II) adsorption onto CMNPs

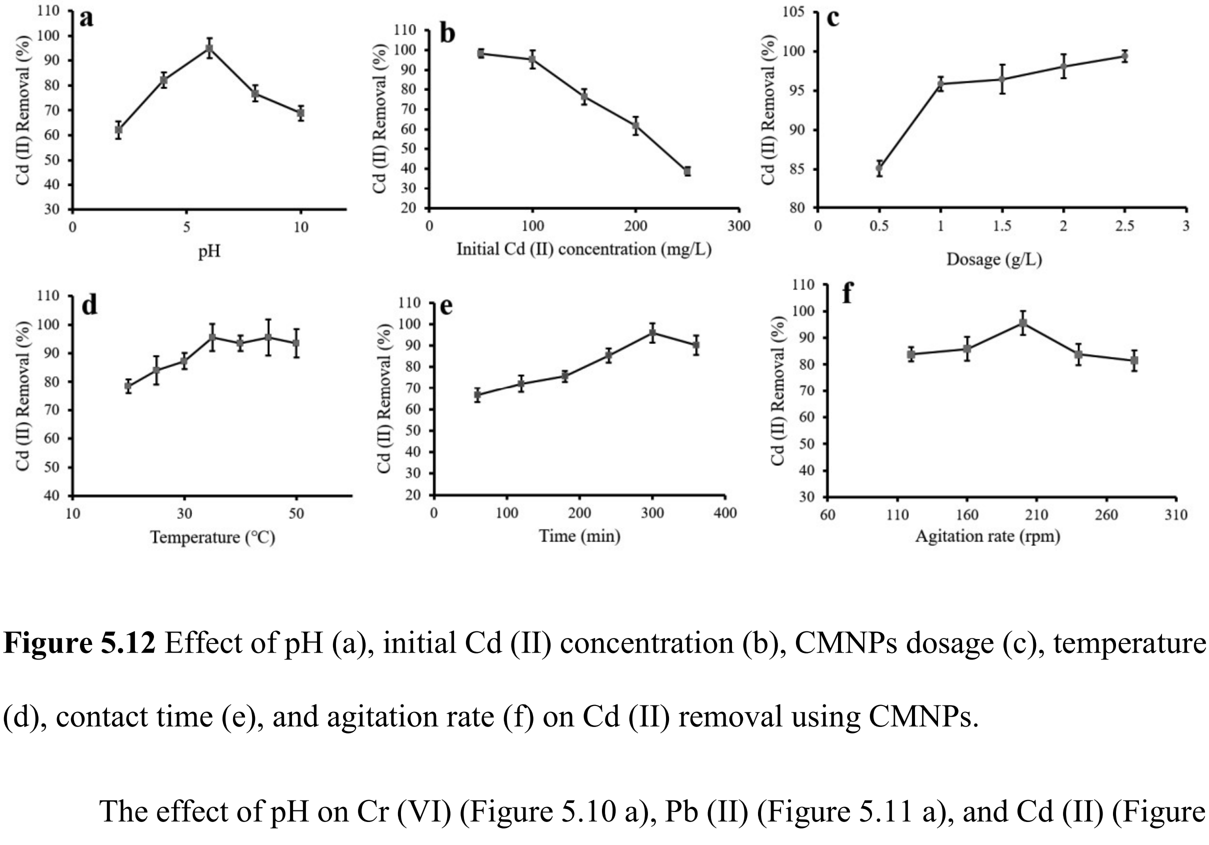

Figure 5.12 Effect of pH (a), initial Cd (II) concentration (b), CMNPs dosage (c), temperature (d), contact time (e), and agitation rate (f) on Cd (II) removal using CMNPs.

The effect of pH on Cr (VI) (Figure 5.10 a), Pb (II) (Figure 5.11 a), and Cd (II) (Figure 5.12 a) removal was observed in range of 2-10. The maximum Cr (VI) removal was achieved at pH 2. The maximum removal of Cr (VI) at pH 2 was due to heavy protonation CMNPs surface, which attracted chromate ions from the liquid phase. Above pH 2, a sharp decrease in the % removal of Cr (VI) (chromate ion) was observed. The rationale behind the decrement in the removal of Cr (VI) ions above pH 2 was sudden deprotonation of CMNPs surface. Dawodu et al., 2020 conducted Cr (VI) biosorption on *Heinsia crinita* seed coat and reported that maximum removal of Cr (VI) was achieved at pH 2. Removal of Pb (II) was increased with the increase in pH up to 6 and maximum Pb (II) removal was achieved at pH 6 (Figure 5.11 a). Further increment in the pH after 6, the removal of Pb (II) continuously decreased. However, lowest removal of Pb (II) was in acidic pH (2-5) range. This is due to the extreme competition for active sites between free hydrogen ions in the liquid medium and positively charged metal ions which is responsible for decrement of Pb (II) adsorption onto CMNPs [Mahmoud et al., 2021]. On other hand, when solution pH increases, the concentration of free hydrogen ions in the solution decreased and thus the competition for active sites declined which favoured the adsorption of Pb (II). Mahmoud et al., 2021 investigated Pb (II) adsorption using chitosan coated MnO_2 nanoparticles and reported that maximum Pb (II) removal was achieved at pH 6 and thereafter, the removal of Pb (II) decreased. The maximum Cd (II) removal was observed at pH 6 (Figure 5.12 a). It was observed that the removal of Cd (II) increased with rise in the solution pH up to 6 and afterwards Cd (II) removal decreased. Kara et al., 2021 performed Cd (II) removal from wastewater using Maleic Anhydride Nanocellulose. Authors reported that Cd (II) removal increased with the surge in pH from 2 to 8. Above pH 8, the Cd (II) removal decreased substantially.

The effect of initial Cr (VI) (Figure 5.10 b), Pb (II) (Figure 5.11 b) and Cd (II) (Figure 5.12 b) ion concentration on the heavy metal removal efficiency of CMNPs was determined by varying the initial metal ion concentration from 50 - 250 mg/L. The maximum Cr (VI), Pb (II) and Cd (II) removal was achieved at 50 mg/L. Above 50 mg/L concentration, a decrease in the percentage removal of heavy metal ions was observed. This decline in removal percentage above 50 mg/L was attributed to the unavailability/ saturation of active sites present on the surface of CMNPs. Mondal and Basu, 2019 also performed the biosorption of Cr (VI) on human hair waste and observed that the removal % of chromium decreased with the increase in initial concentration of metal ion. Farghali et al., 2013 investigated Pb (II) removal using copper oxide nanostructures and reported that Pb (II) removal decreased with elevation in Pb (II) concentration. Devi et al., 2017 investigated Cd (II) removal from water by using CNSR functionalized Fe_3O_4 magnetic nanoparticles. Authors performed Cd (II) removal study at initial metal ion concentration of 50 mg/L and 100 mg/L. The maximum Cd (II) removal was achieved 50 mg/L.

The effect CMNPs dose on Cr (VI) (Figure 5.10 c), Pb (II) (Figure 5.11 c) and Cd (II) (Figure 5.12 c) removal was studied in range of 0.5 to 2.5 g/L. The removal of heavy metal ions increased with the escalation in the CMNPs dose and maximum heavy metal removal was achieved at 2.5 g/L. The increase heavy metal removal with the increase in CMNPs dosage was due to rise in the number of active sites available for biosorption [Cardoso et al., 2011]. Gupta and Rastogi, 2009 also investigated the biosorption of Cr (VI) on raw and acid-treated green alga *Oedogoniumhatei* from aqueous solutions and confirmed that the removal of Cr (VI) increased with the increase in biosorbent dosage up to a certain limit. Gaur et al., 2018 investigated behaviour of Pb (II) adsorption using soya bean waste and it was observed that removal of Pb (II) was influenced with increase in adsorbent dosage. Al-Qahtani, 2017 investigated Cd (II) removal from aqueous solution by using zero valent silver nanoparticles and observed effect of adsorbent dosage (10 to 100 mg/L) on Cd (II) removal. Authors reported that Cd (II) removal increased with the rise in adsorbent dosage and maximum Cd (II) removal was observed at 100 mg/L.

Cr (VI), Pb (II) and Cd (II) removal using CMNPs was also performed at various temperature range from 20 - 50ºC. The Cr (VI) removal increased with the rise in temperature from 20 to 50ºC (Figure 5.10 d). Finally, maximum Cr (VI) removal was observed at temperature 50ºC which indicated endothermic nature of Cr (VI) adsorption onto CMNPs. Kakavandi et al., 2014 also reported that Cr (VI) removal increased with the increase in temperature from 20 to 50ºC. Authors studied Cr (VI) adsorption onto activated carbon modified by zero valent ion and silver bimetallic nanoparticles. The removal of Pb (II) increased quickly up to 35°C and further it became slow from 35 to 50°C (Figure 5.11 d). The maximum removal of Pb (II) was achieved at 50°C. Increased Pb (II) removal with the increase solution temperature indicated endothermic adsorption. The more number of active sites on the adsorbent were exposed at higher temperature which were responsible for increased Cd removal [Saleem et al., 2007]. Fato et al., 2019 performed simultaneous removal of multiple heavy metal ions including Pb (II) using magnetite nanoparticles from river water and observed that removal of metal ions increased with upsurge in solution temperature from 5 - 45°C and maximum metal ion removal was achieved at 45°C. The removal of Cd (II) increased with surge in solution temperature and maximum Cd (II) removal was observed at 50°C (Figure 5.12 d). This indicated that Cd (II) removal was temperature dependent. The active site on the adsorbent were more exposed at higher temperature which led to increased Cd (II) removal [Saleem et al., 2007]. Similar investigation was also reported by Javadian et al., 2015. Authors reported that adsorption of Cd (II) increased with rise solution temperature from 20-45°C and maximum Cd (II) adsorption was reported at 45°C.

The effect of contact time was studied in the range of 60-360 minutes. The maximum Cr (VI) (Figure 5.10 e), Pb (II) (Figure 5.11 e) and Cd (II) (Figure 12 e) removal was achieved at 300 minutes (Figure 5.10 e). After 300 minutes there was no increment in the adsorption. This was attributed to the fact that all the active sites on CMNPs surface were saturated at 300 minutes and hence no or negligible adsorption took place thereafter. Similar kind of results were reported by Gupta and Rastogi, 2008. Authors carried out the biosorption experiment on non-living biomass *Oedogonium* sp. and *Nostoc* sp. and found that maximum removal of Cr (VI) achieved between 60 to 70 minutes. The Pb (II) removal on CMNPs continuously increased with surge in contact time and maximum Pb (II) removal was achieved at 300 minutes (Figure 5.11 e). Moyo et al., 2013 investigated Pb (II) removal by using maize tassel based activated carbon and authors reported that Pb (II) removal increased with increase in agitation time and equilibrium was achieved at 60 minutes. Givianrad et al., 2013 carried out Cd (II) adsorption in range of 5-240 minutes and equilibrium was achieved in 90 minutes.

Agitation is also an important parameter for heavy metal adsorption and it was evaluated during Cr (VI) (Figure 5.10 f), Pb (II) (Figure 5.11 f) and Cd (II) (Figure 5.12 f) adsorption onto CMNPs at various agitation rate in the range of 120-280 rpm. Results revealed that removal of Cr (VI), Cd (II) and Pb (II) increased with rise in agitation rate up to 200 rpm and thereafter there was no increment. This increment was due to the increase in turbulence in aqueous phase which resulted higher collision rate between CMNPs and metal ion and reduced thickness of boundary layer surrounding the CMNPs [Parvathi and Nagendran, 2007]. Kumar and Jena, 2017 studied the effect of agitation rate on the removal of Cr (VI) using chemical activated $ZnCl_2$ nanoparticles. Authors concluded that % removal of Cr (VI) increased with the rise in agitation rate from 90 - 150 rpm and there was no effect on Cr (VI) adsorption above 150 rpm. Inyinbor et al., 2020 also observed similar kind of result for Cu (II) adsorption using usea modified crop residue. Murithi et al., 2014 investigated Cd (II) adsorption using Hyacinth biomass and observed effect of agitation rate in the range of 0 to 200 rpm. The maximum adsorption was reported at 175 rpm.

5.3.2 Isotherm

Isotherm study of Cr (VI), Pb (II) and Cd (II) biosorption were performed at 50-200 mg/L initial metal ion concentration and at 20-50 °C. The biosorption data of Cr (VI), Pb (II), Cd (II) in single and ternary metal ion system on CMNPs were fitted in the Langmuir, Freundlich, Temkin and Halsey isotherms are shown in Figure 5.13, 5.14, 5.15 and 5.16.

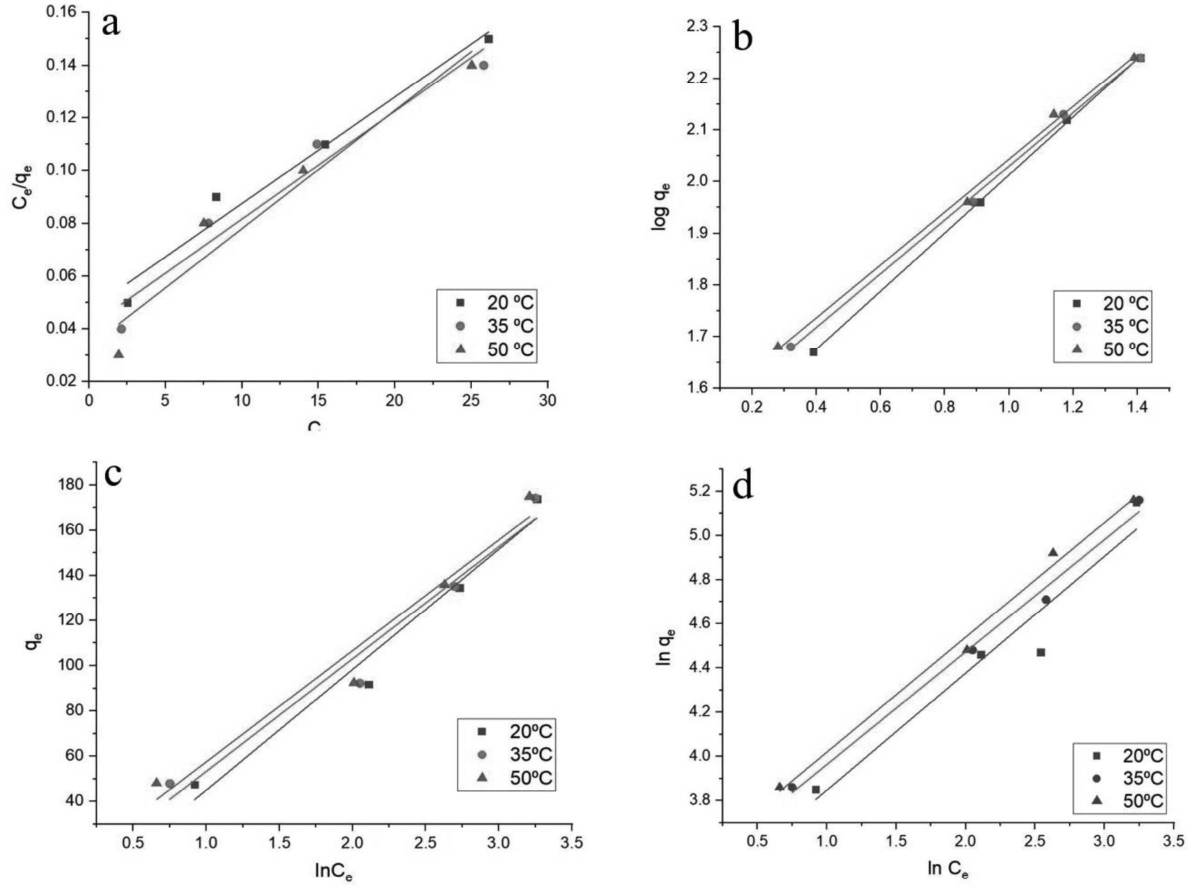

Figure 5.13 Langmuir (a), Freundlich (b), Temkin (c), and Halsey (d) isotherms of Cr (VI) biosorption CMNPs.

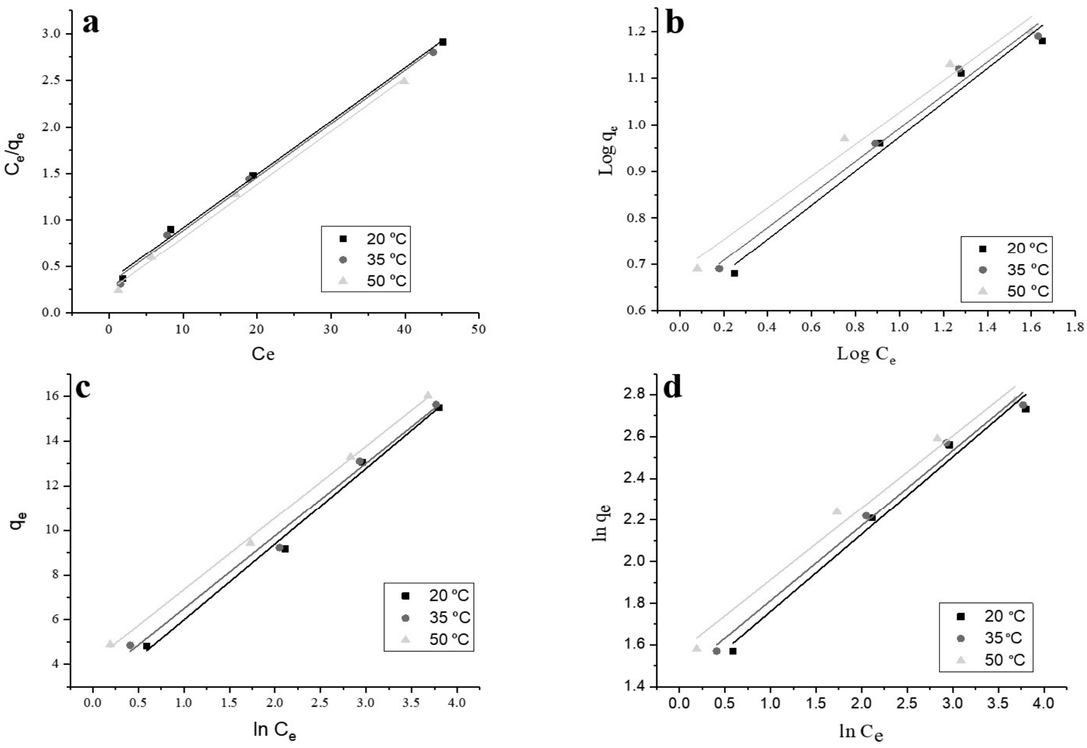

Figure 5.14 Langmuir (a), Freundlich (b), Temkin (c), and Halsey (d) isotherms of Pb (II) biosorption CMNPs.

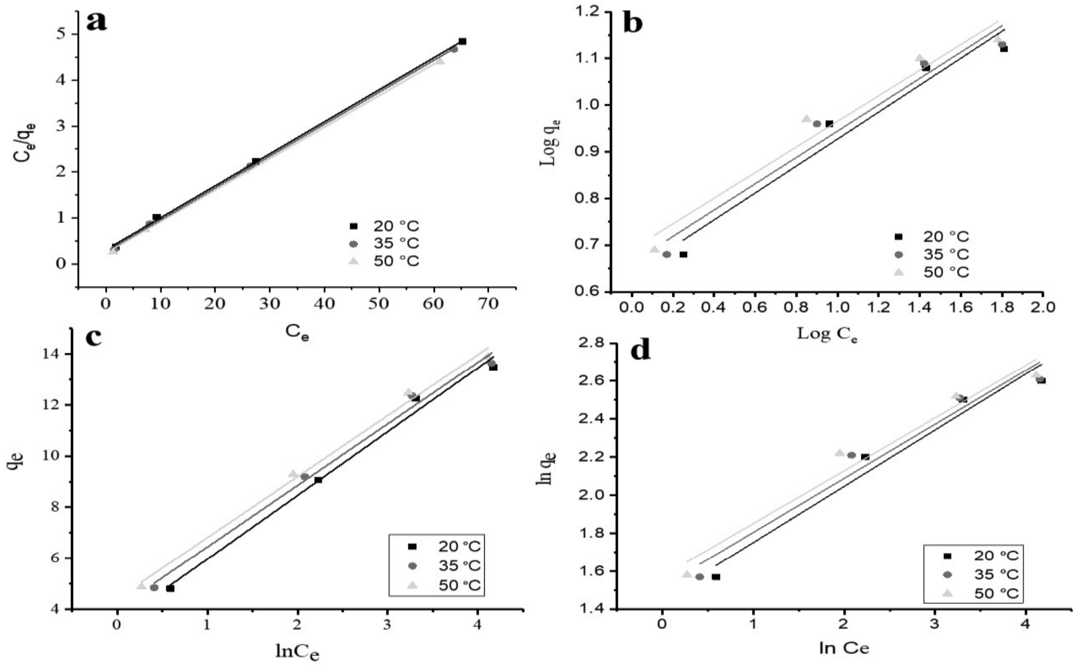

Figure 5.15 Langmuir (a), Freundlich (b), Temkin (c), and Halsey (d) isotherms of Cd (II) biosorption on the surface of CMNPs.

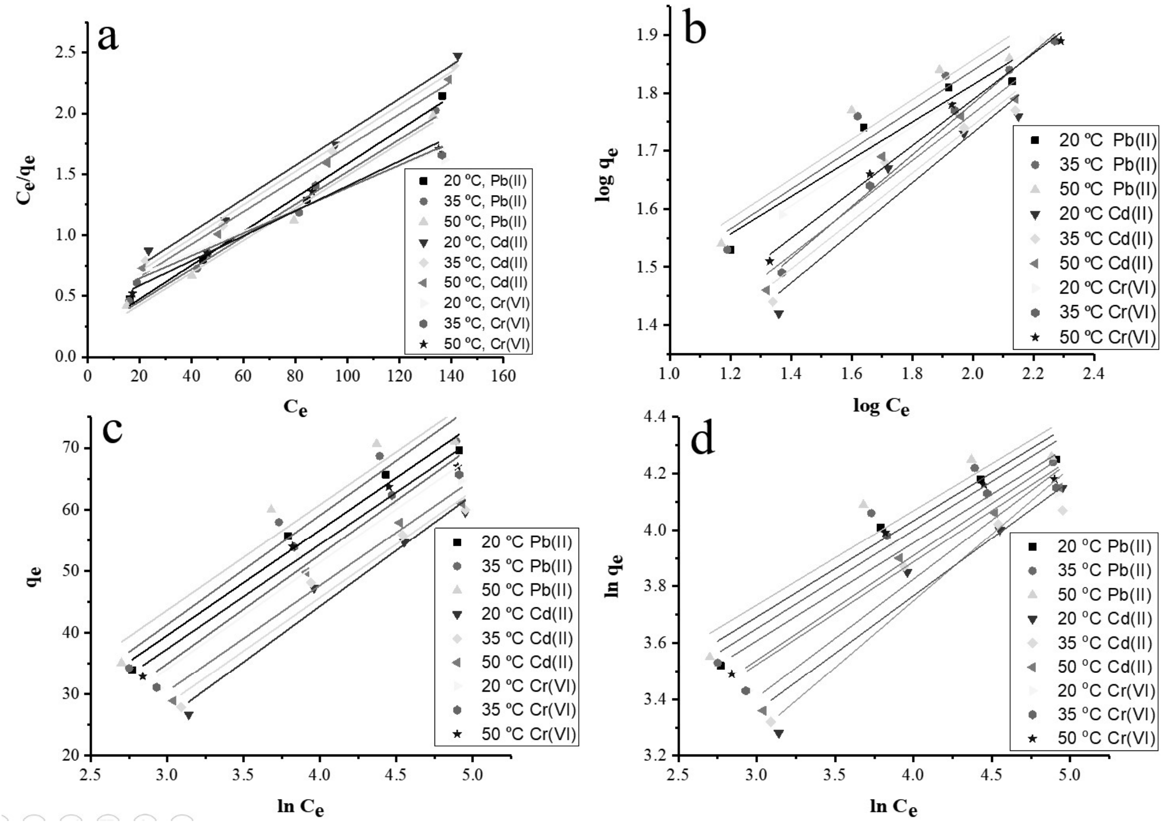

Figure 5.16 Langmuir (a), Freundlich (b), Temkin (c), and Halsey (d) isotherms study of Cr (VI), Cd (II) and Pb (II) biosorption in ternary metal ion system onto CMNPs

The isotherm parameters were calculated from the graphs of isotherm models and tabulated in the Table 5.2, 5.3, 5.4 and 5.5.

Table 5.2 Isotherms parameters of Cr (VI) biosorption on CMNPs

Isotherms	Parameters	20ºC	35ºC	50ºC
Langmuir	B	0.05	0.04	0.03
	Q^0	3.60×10^{-3}	4.30×10^{-3}	4.70×10^{-3}
	R^2	0.97	0.95	0.94
	RSS	1.46×10^{-4}	2.50×10^{-4}	3.58×10^{-4}
Freundlich	*k_f*	1.45	1.51	1.53
	N	0.56	0.52	0.51

	R^2	0.99	0.99	0.99
	RSS	5.16×10^{-5}	3.21×10^{-4}	5.42×10^{-4}
Temkin	A_T	-8.28	3.61	8.41
	b_T	53.30	49.70	49.10
	R^2	0.96	0.96	0.96
	RSS	279.08	315.28	348.63
Halsey	K_H	0.52	0.50	0.51
	n_H	3.31	3.45	3.49
	R^2	0.93	0.99	0.99
	RSS	5.16×10^{-2}	6.84×10^{-3}	7.36×10^{-3}

Table 5.3 The isotherm parameters of Pb (II) biosorption at various temperature

Isotherms	Parameters	20ºC	35ºC	50ºC
Langmuir	B	0.34	0.031	0.23
	Q^0	0.06	0.06	0.06
	R^2	0.99	0.99	0.99
	RSS	0.013	0.016	0.010
Freundlich	k_f	0.36	0.35	0.34
	N	0.60	0.63	0.68
	R^2	0.98	0.98	0.98
	RSS	0.002	0.0018	0.0029
Temkin	A_T	2.59	3.23	4.14
	b_T	3.39	3.25	3.20
	R^2	0.99	0.98	0.99

	RSS	0.56	0.67	0.09
Halsey	K_H	0.37	0.36	0.34
	n_H	1.38	1.45	1.56
	R^2	0.98	0.98	0.98
	RSS	0.012	0.009	0.015

Table 5.4 The isotherm parameters of Cd (II) biosorption

Isotherms	Parameters	20ºC	35ºC	50ºC
Langmuir	B	0.307	0.26	0.23
	Q^0	0.0696	0.0694	0.0685
	R^2	0.99	0.99	0.99
	RSS	0.0084	0.0071	0.0098
Freundlich	k_f	0.29	0.28	0.27
	N	0.63	0.66	0.69
	R^2	0.95	0.95	0.95
	RSS	0.0054	0.0051	0.0052
Temkin	A_T	3.47	4.03	4.42
	b_T	2.49	2.40	2.38
	R^2	0.98	0.98	0.99
	RSS	0.45	0.40	0.32
Halsey	K_H	0.29	0.28	0.27
	n_H	1.45	1.52	1.57
	R^2	0.96	0.96	0.96
	RSS	0.023	0.025	0.025

Table 5.5 Isotherm parameters of Cr (VI), Cd (II) and Pb (II) biosorption in ternary metal ion system

Metal	**Isotherms**	**Parameters**	**20ºC**	**35ºC**	**50ºC**
Pb (II)	Langmuir	B	0.20	0.19	0.16
		Q^0	1.4×10^{-2}	1.3×10^{-2}	1.2×10^{-2}
		R^2	0.99	0.98	0.98
		RSS	1.3×10^{-2}	1.4×10^{-2}	1.6×10^{-2}
	Freundlich	k_f	0.32	0.34	0.35
		N	1.17	1.15	1.17
		R^2	0.92	0.90	0.91
		RSS	4.2×10^{-3}	5.7×10^{-3}	5.4×10^{-3}
	Temkin	A_T	-11.60	-11.90	-7.77
		b_T	17.06	17.74	17.14
		R^2	0.97	0.95	0.91
		RSS	19.35	41.65	68.80
	Halsey	K_H	0.3475	0.3406	0.3339
		n_H	2.60	2.67	2.73
		R^2	0.95	0.90	0.88
		RSS	1.49×10^{-2}	3.23×10^{-2}	3.74×10^{-2}
	Langmuir	B	0.47	0.43	0.39
		Q^0	1.37×10^{-2}	1.41×10^{-2}	1.33×10^{-2}
		R^2	0.98	0.99	0.99
		RSS	1.6×10^{-2}	9.3×10^{-3}	7.9×10^{-3}

Cd (II)	Freundlich	k_f	0.43	0.41	0.40
		N	0.86	0.92	0.95
		R^2	0.91	0.92	0.93
		RSS	6.2×10^{-3}	5.1×10^{-3}	4.1×10^{-3}
	Temkin	A_T	-28.10	-23.59	-21.1
		b_T	18.10	17.32	17.19
		R^2	0.96	0.96	0.95
		RSS	21.06	21.28	27.28
	Halsey	K_H	0.47	0.40	0.41
		n_H	1.86	2.13	2.15
		R^2	0.95	0.97	0.95
		RSS	2.0×10^{-2}	3.02×10^{-2}	2.11×10^{-2}
Cr (VI)	Langmuir	B	0.50	0.46	0.38
		Q^0	8.8×10^{-3}	9.2×10^{-3}	1.02×10^{-2}
		R^2	0.93	0.96	0.98
		RSS	7.6×10^{-3}	1.05×10^{-2}	4.5×10^{-3}
	Freundlich	k_f	0.34	0.39	0.44
		N	1.12	0.89	0.99
		R^2	0.99	0.99	0.99
		RSS	2.77×10^{-4}	5.85×10^{-4}	7.55×10^{-4}
	Temkin	A_T	-17.74	-18.01	-13.48
		b_T	17.28	17.66	16.95
		R^2	0.96	0.95	0.97
		RSS	24.57	36.32	20.29

Halsey	K_H	0.363	0.370	0.346
	n_H	2.43	2.42	2.26
	R^2	0.91	0.89	0.92
	RSS	2.88×10^{-2}	3.62×10^{-2}	2.34×10^{-2}

The highest R^2 value together with the lowest RSS for Cr (VI) biosorption in single (Table 5.2) and ternary (Table 5.5) metal ion system was recorded for the Freundlich model as compared to other isotherms. This not only demonstrated the suitability of Freundlich isotherm but also proved that biosorption of Cr (VI) was in multilayers and the surface of CMNPs was heterogeneous. Increase in k_f value from 1.45 to 1.53 mg/g for single and 0.34 to 0.44 mg/g for ternary metal ion system with the increase in solution temperature from 20°C to 50°C indicated that adsorption was favorable at high temperature. The value of n for Cr (VI) adsorption was 0.56, 0.52 and 0.51 for single, and 1.12, 0.89 and 0.99 for ternary metal ion system at temperature 20, 35 and 50°C which also indicated towards favorable adsorption of Cr (VI) onto CMNPs surface. Tho et al., 2021 performed multiple heavy metal (As^{3+}, Cd^{2+}, Cr^{6+} and Pb^{2+}) adsorption by biochar modified with ZnO nanoparticles. Authors reported that Freundlich isotherm best fitted in the adsorption data. Abatan et al., 2020 performed Cr (VI) and Cd (II) adsorption by eggshells powder. Authors reported that adsorption of Cr (VI) and Cd (II) onto eggshells powder was described by Freundlich isotherm. Fu et al., 2015 performed Cr (VI) decontamination using sepiolite-supported nanoscale zero-valent iron. The authors concluded that Freundlich isotherm had higher goodness of fit compared to other isotherms. Zheng et al., 2019 attempted Cr (VI) adsorption using 4-vinyl pyridine decorated magnetic chitosan biopolymer and reported similar kind of results. Aslani et al., 2018 reported that experimental data of Cr (VI) adsorption on to magnetic nanoparticles of chitosan modified with polyhexamethylene biguanide well fitted in Freundlich isotherm. Ghanbarian et al., 2017 pointed out that Cr (VI) adsorption on to magnetic cellulose and amine modified cellulose nanoparticles was of multilayer type and the surface of adsorbent was heterogeneous. Similar results were observed by Li et al., 2016 while performing Cr (VI) adsorption on the magnetic mesoporous composite**.**

The higher R^2 values and lower RSS of Pb (II) (Table 5.3), Cd (II) (Table 5.4) in single metal ion system and ternary (Table 5.5) indicated that Langmuir isotherm was best fitted in the adsorption data as compared to other isotherms. Langmuir isotherm model assumes rapid reduction in the intermolecular forces between adsorbate molecules, which is responsible for monolayer coverage of adsorbate molecules on the adsorbent's surface [Ossman and Mansour, 2013]. Suitability of Langmuir isotherm also indicates the specific homogeneous distribution of adsorbate molecules on the adsorbent's surface [Ossman and Mansour, 2013]. In the present study it was concluded that Pb (II) and Cd (II) ions in single and ternary metal ion system were adsorbed in monolayer on the surface of CMNPs surface. Moreover, CMNPs surface was structurally homogeneous where all biosorption site are identical and energetically equivalent. Wang et al., 2019 investigated Cd (II) adsorption by modified rice straw and reported that Langmuir isotherm better fitted in the adsorption data. Givianrad et al., 2013 synthesized nanocomposite, silica aerogel, activated carbon for adsorption of Cd (II) from the aqueous solution. Authors reported that Langmuir isotherm best fitted in the adsorption data which indicated monolayer adsorption of Cd (II) on to homogeneous surface of nanocomposite, silica aerogel and activated carbon.

Huang et al., 2017 studied the biosorption of Pb (II), Zn (II) and Cu (II) ions from water by silicate hierarchical nanoparticles and authors reported that Langmuir isotherm best fitted in the adsorption data. Safatian et al., 2019 investigated Pb (II) from wastewater by hydroxyapatite nanoparticles and reported that Langmuir isotherm was best fitted in the adsorption data. Manyangadze et al., 2020 investigated Pb (II) adsorption by using silica based nano adsorbent and reported Langmuir isotherm best fitted as compared to Freundlich isotherm model.

Fato et al., 2019 investigated multiple heavy metals (Pb^{2+}, Cd^{2+}, Cu^{2+} and Ni^{2+}) adsorption using Fe_3O_4 and reported that Langmuir isotherm model best fitted in the adsorption data. El-Dib et al., 2019 investigated the adsorption of Cd^{2+}, Pb^{2+} and Zn^{2+} onto magnetite nanoparticles and observed that Cd^{2+} and Pb^{2+} adsorption data was best fitted in the Langmuir isotherm. Asuquo et al., 2017 investigated the Cd^{2+} and Pb^{2+} adsorption using mesoporous activated carbon. Authors reported that Langmuir isotherm best fitted in the adsorption data. Tang et al., 2018 observed Cd^{2+} and Pb^{2+} adsorption by using amino and thiol functionalized activated carbon and authors reported that Langmuir isotherm was most suitable to describe adsorption.

5.3.3 Kinetics

Kinetic model such as PFO, PSO and Elovich were studied for biosorption of Cr (VI), Pb (II), Cd (II) in single and ternary metal ion system and results are shown in Figure 5.17, 5.18, 5.19 and 5.20.

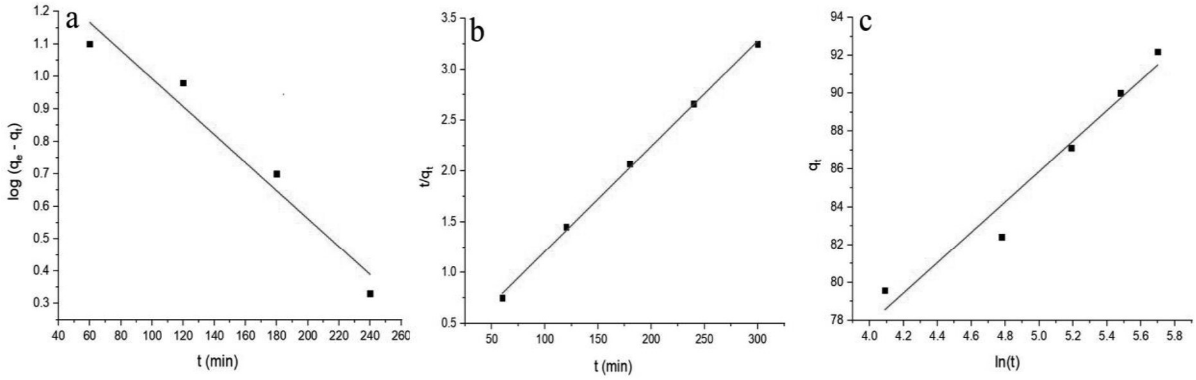

Figure 5.17 PFO (a), PSO (b) and Elovich (c) kinetic models of Cr (VI) biosorption onto CMNPs.

.

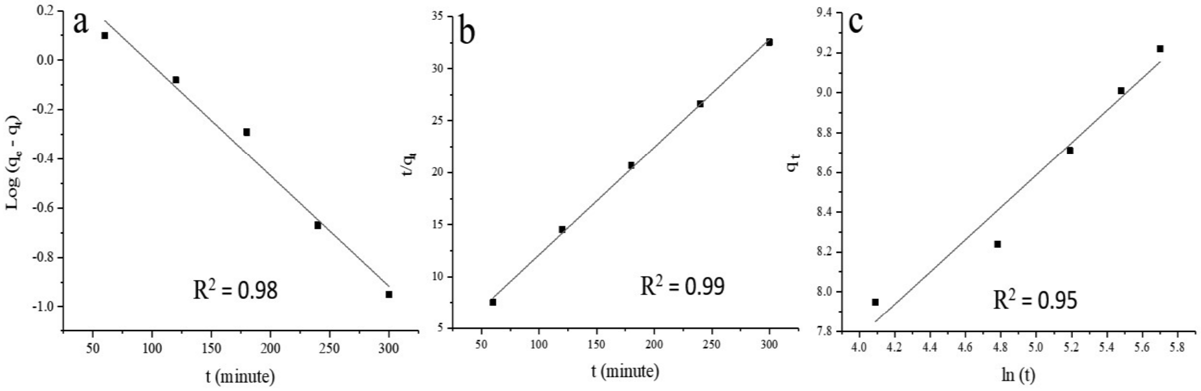

Figure 5.18 PFO (a), PSO (b) and Elovich (c) kinetic models of Pb (II) biosorption onto CMNPs.

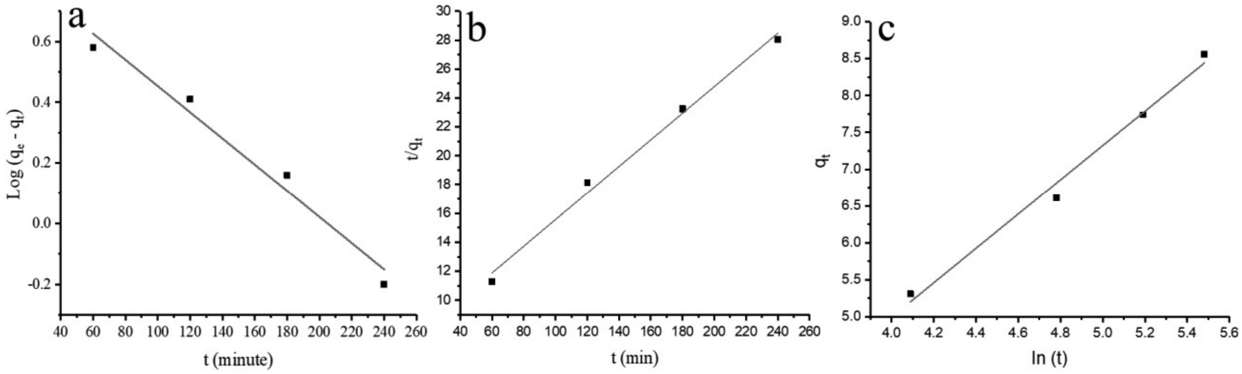

Figure 5.19 PFO (a), PSO (b) and Elovich (c) kinetics of Cd (II) biosorption onto CMNPs.

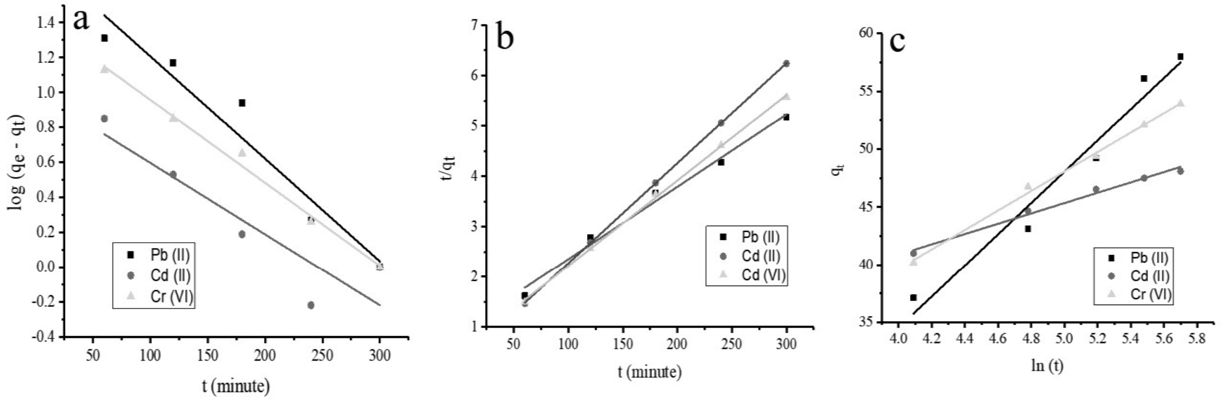

Figure 5.20 PFO (a), PSO (b), and Elovich (c) kinetics of Pb (II), Cd (II) and Cr (VI) biosorption in ternary metal ion system.

The kinetic parameters such as K_s, q_e, k'_2, q_e', α, β, and R^2 for Cr (VI), Pb (II) and Cd (II) biosorption onto CMNPS in single and ternary metal ion system were calculated from the slope and intercept of several kinetic model and are tabulated in the Table 5.6, 5.7, 5.8 and 5.9.

Table 5.6 Kinetics of Cr (VI) biosorption

PFO				**PSO**				**Elovich kinetic**			
k_s	q_e	R^2	RSS	k'_2	h	R^2	RSS	α	β	R^2	RSS
4.00×10^{-3}	1.42	0.95	1.5×10^{-2}	0.17	0.01	0.99	0.00	8.04	45.64	0.95	4.49

Table 5.7 Kinetics of Pb (II) biosorption

PFO				**PSO**				**Elovich kinetic**			
k_s	q_e	R^2	RSS	k'_2	q_e'	R^2	RSS	α	β	R^2	RSS
4.4×10^{-3}	0.42	0.98	0.01	1.76	0.10	0.99	4.8×10^{-3}	0.81	4.52	0.95	0.49

Table 5.8 Kinetic of Cd (II) biosorption on to CMNPs

PFO				PSO				Elovich kinetic			
k_s	q_e	R^2	RSS	k'_2	q'_e	R^2	RSS	α	β	R^2	RSS
-4.3×10^{-3}	0.88	0.97	0.90	6.35	0.09	0.99	0.04	2.32	-4.32	0.98	0.66

Table 5.9 Kinetic parameters of Pb (II), Cd (II) and Cr (VI) biosorption in ternary metal ion system

Metal	PFO				PSO				Elovich kinetic			
	k_s	q_e	R^2	RSS	k'_2	q'_e	R^2	RSS	α	β	R^2	RSS
Pb(II)	-5.8×10^{-3}	1.79	0.93	0.79	0.91	1.4×10^{-2}	0.99	0.08	13.5	-19.45	0.96	10.29
Cd(II)	-4.0×10^{-3}	1.00	0.93	0.12	0.28	2.0×10^{-2}	0.99	0.05	4.45	23.08	0.98	0.43
Cr(VI)	-4.7×10^{-3}	1.43	0.98	0.68	0.51	1.6×10^{-2}	0.99	0.09	8.39	6.08	0.99	0.40

Based on the higher R^2 and lower RSS value, PSO kinetic model best fitted in the biosorption data of Cr (VI) (Table 5.6) Pb (II) (Table 5.7) and Cd (II) (Table 5.8) in single and ternary metal ion system (Table 5.9). This indicated that adsorption of Pb (II), Cd (II) and Cr (VI) on the surface of CMNPs followed chemisorption in both single and ternary metal ion system. Egbosiuba et al., 2021 investigated Cr (VI), Ni (II), Fe (II) and Cd (II) adsorption by KIAgNPs decorated MWCNTs nano adsorbent. Authors reported that adsorption of Cr (VI), Cr (VI), Ni (II), Fe (II) and Cd (II) was best fitted in the pseudo second order kinetics. This revealed chemisorption temperament of Cr (VI), Ni (II), Fe (II) and Cd (II) adsorption. Mohamed et al., 2019 performed removal of Cr (VI) and Cd (VI) by using *Padina gymnospora* waste. Authors reported that Pseudo second order kinetic model best fitted in the experimental data to describe Cr (VI) and Cd (II) adsorption. This indicated that adsorption of Cr (VI) and Cd (II) followed chemisorption. Roy and Bhattacharya (2013) investigated ternary metal ions adsorption using y-Fe_3O_4 nanotubes and reported that adsorption data of ternary heavy metal system was best fitted in the pseudo second order kinetic model.

Kara and Demirbel, 2012 studied the adsorption of Cr (VI) on the magnetic-poly (divinylbenzene-1-vinylimidazole) microbeads and observed that the adsorption followed pseudo-second order kinetic model. Authors also confirmed the chemisorption mode of Cr (VI) adsorption. Wang et al., 2018 concluded that adsorption of Cr (VI) on Fe_3O_4 nanoparticle-coated mushroom followed pseudo-second order model. Samuel et al., 2019 reported that Cr (VI) adsorption on the surface of chitosan grafted graphene oxide nanocomposite followed pseudo-second order kinetics. Subedi et al., 2019 did Cr (VI) adsorption on graphene oxide modified magnetic chitosan and concluded that pseudo-second order model had a better goodness of fit as compared to other rate determining models.

Zaidi et al., 2021 investigated the Pb (II) adsorption using copper oxide nanoparticle. Authors studied kinetics and reported that pseudo second order kinetic model was best fitted in the adsorption data. Sharma et al., 2018 investigated Pb (II) and Hg (II) adsorption using Ceria Nanoparticles and reported that Pseudo second order kinetic best fitted in the experimental data. Batool et al., 2018 performed kinetic study for adsorption of Cd (II) on to stem of *Saccharum arundinaceum.* Authors reported that pseudo second order kinetic model best fitted in the adsorption data. Kumar et al., 2010 investigated thermodynamics and kinetics of Cd (II) removal by rice husk and reported that pseudo second order kinetic model was best fitted in the adsorption data to describe chemisorption type adsorption Cd (II) on to rice husk surface.

5.3.4 Thermodynamics

The thermodynamic study of Cr (VI), Pb (II) and Cd (II) biosorption on to CMNPs in single and ternary metal ion system was investigated in range of 20 to 50 °C. The value of ΔS° and ΔH° were determined from intercept and slope of the plot (Figure 5.21) between lnk_c versus 1/T.

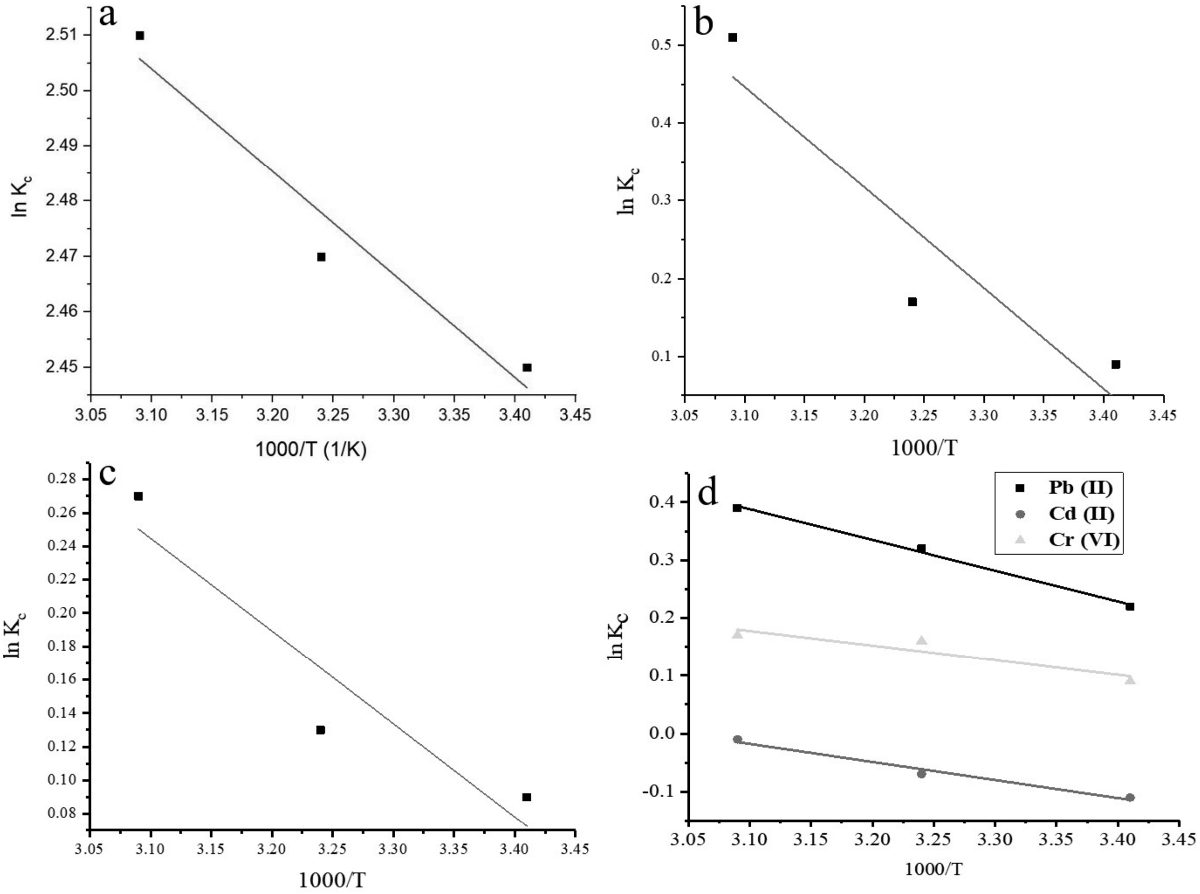

Figure 5.21 Thermodynamics of Cr (VI) (a), Pb (II) (b), Cd (II) (c) and ternary (d) metal ion system on to CMNPs.

The thermodynamic parameters were calculated and listed in the Table 5.10, 5.11, 5.12 and 5.13.

Table 5.10 Thermodynamic data for biosorption of Cr (VI) on to CMNPs

T (°C)	ΔG° (J mol^{-1})	ΔH° (J mol^{-1})	ΔS° (J K^{-1} mol^{-1})
20	-5854.22	2891.03	29.85

35	-6301.93
50	-6749.64

Table 5.11 Thermodynamic data for biosorption of Pb (II) on to CMNPs

T (^{o}C)	**ΔG^o (kJ mol^{-1})**	**ΔH^o (kJ mol^{-1})**	**ΔS^o (J K^{-1} mol^{-1})**
20	-0.21		
35	-0.43	4.45	1.29
50	-1.37		

Table 5.12 Thermodynamic data for biosorption of Cd (II) on to CMNPs

T (^{o}C)	**ΔG^o (KJ mol^{-1})**	**ΔH^o (K J mol^{-1})**	**ΔS^o (J K^{-1} mol^{-1})**
20	-0.24		
35	-0.33	1.96	0.55
50	-0.72		

Table 5.13 Thermodynamic parameters of Pb (II), Cd (II) and Cr (VI) biosorption on to CMNPs in ternary metal ion system

Heavy Metal	**T (^{o}C)**	**ΔG^o (kJ mol^{-1})**	**ΔH^o (kJ mol^{-1})**	**ΔS^o (J k^{-1} mol^{-1})**
Pb (II)	20	-8.25	0.53	2.03
	35	-8.30		
	50	-8.31		
Cd (II)	20	-0.26	0.31	0.94
	35	-0.17		
	50	-0.27		

Cr (VI)	20	-0.22	0.25	0.96
	35	-0.41		
	50	-0.46		

The thermodynamic data of Cr (VI), Cd (II) and Pb (II) biosorption in single and ternary metal complex was compared with literature (Table 5.14).

Table 5.14 Comparative thermodynamic data present study and literature

Heavy Metal	**Adsorbent**	**ΔG^o**	**ΔH^o**	**ΔS^o**	**Behaviour of heavy metal adsorption**	**References**
Cr (VI)	Chemically activated nutshell	Negative	Positive	Positive	Spontaneous, and endothermic adsorption	Kumar and Jena, 2017
Cd (II), Cu (II), and Pb (II)	Natural clay	Negative	Positive	Positive	Spontaneous, and endothermic adsorption	Abbou et al., 2021
Cd (II) and Pb (II)	Turkish illitic clay	Negative	Positive	Positive	Spontaneous, and endothermic adsorption	Ozdes et al., 2011

Cr (VI)	Activated carbon from leaves of *Ficus nitida*	Negative	Positive	Positive	Spontaneous, and endothermic adsorption	Ali IH, Alrafai, 2016
Cr (VI)	*Ficus carica* biosorbent	Negative	Positive	Positive	Spontaneous, and endothermic adsorption	Gupta et al., 2013
Cd (II)	*Nannochloropsis oculata* biomass	Negative	Negative	Positive	Feasible, spontaneous and exothermic	Kaparapu and Krishna Prasad, 2018
Pb(II)-Cd(II)-Cr(VI) Ternary		Negative	Positive	Positive	Spontaneous, and endothermic adsorption	Present study
Pb (II)-Single		Negative	Positive	Positive	Spontaneous, and endothermic adsorption	Present study
Cd (II)-Single		Negative	Positive	Positive	Spontaneous, and endothermic adsorption	Present study

Cr (VI)-Single		Negative	Positive	Positive	Spontaneous, and endothermic adsorption	Present study

The thermodynamic parameters of Cr (VI) (Table 5.10), Pb (II) (Table 5.11), Cd (II) (Table 5.12) and ternary metal ion system (Table 5.13) showed negative ΔG^o, positive ΔH^o and ΔS^o for single and ternary metal ion system. The negative ΔG^o and positive ΔH^o showed spontaneous and endothermic biosorption of Cr (VI), Pb (II) and Cd (II) in single and ternary metal ion system. Additionally, ΔG^o became more negative with increase in temperature from 20 to 50°C, which revealed the favourable biosorption of Pb (II), Cd (II) and Cr (VI) at higher temperature. The positive value of ΔS^o revealed increased randomness at metal solution-CMNPs interface. Kumar and Jena, 2017 investigated Cr (VI) adsorption by chemically activated nutshell and observed that Cr (VI) adsorption had negative ΔG^o and positive ΔH^o which indicated spontaneous and endothermic adsorption of Cr (VI). Abbou et al., 2021 investigated multiple metal such as Cd (II), Cu (II), and Pb (II) adsorption on natural clay. Authors reported that multiple metal adsorption was spontaneous and endothermic. Ozdes et al., 2011 performed adsorption of Cd (II) and Pb (II) by using Turkish illitic clay and reported Cd (II) and Pb (II) adsorption was spontaneous and endothermic.

Saha et al., 2013 performed adsorption of Cr (VI) on *Citrus limetta* peel powder. The authors reported that adsorption of Cr (VI) on *Citrus limetta* peel was spontaneous and endothermic. Zhu et al., 2018 carried out the Cr (VI) adsorption onto nanoscale zero-valent iron/nickel and observed that adsorption was spontaneous and endothermic. Ren et al., 2017 tested Cr (VI) removal efficiency of porous magnetite nanoparticles and concluded that adsorption was endothermic and spontaneous. Ekop and Eddy, 2009 investigated the thermodynamics of Pb (II) adsorption onto human hair based adsorbent and reported Pb (II) adsorption was endothermic and spontaneous. Manyangadze et al., 2020 also performed the Pb (II) adsorption by using nano silica spheres and reported the negative ΔG° and positive ΔH° which indicated spontaneous and endothermic adsorption. Mahdavi et al., 2020 investigated Pb (II) adsorption by using SnO_2 and WO_3 nanoparticle and reported that adsorption was spontaneous. Kumar et al., 2010 investigated thermodynamic and kinetic study of Cd (II) adsorption on to rice husk. Authors observed negative ΔG° which depicted the spontaneous reaction. Positive ΔH° indicated endothermic reaction.

5.3.5 Dimensionless number and diffusivity coefficients

In the present study, the value of N_k was observed between 10^{-3} and 10^{1} which elucidated that adsorption was mixed diffusion and transfer controlled for Cr (VI), Cd (II) and Pb (II) in single and ternary metal ion system. The dimensionless numbers and diffusivity coefficients were calculated for biosorption data and are shown in Table 5.15.

Table 5.15 Dimensionless numbers and diffusivity coefficients for heavy metal ions in single and ternary metal ion system.

Heavy metal ions	**φ**	**λ**	**N_k**	**D_F**	**D_P**
Cr (VI)-single	9966.49	7.20×10^{-4}	5.03	1.87×10^{-13}	1.91×10^{-12}
Pb (II)-single	9998.59	6.03×10^{-4}	5.08	2.30×10^{-13}	1.91×10^{-12}
Cd (II)-single	9754.59	8.82×10^{-4}	5.26	1.46×10^{-13}	1.91×10^{-12}
Cr (VI)-ternary	5730.81	2.49×10^{-3}	4.48	1.79×10^{-14}	1.91×10^{-12}
Cd (II)-ternary	5198.92	2.50×10^{-3}	3.29	1.47×10^{-14}	1.91×10^{-12}
Pb (II)-ternary	6269.19	2.44×10^{-3}	4.09	2.19×10^{-14}	1.91×10^{-12}

Higher value of N_k results in enhanced biosorption of Cr (VI) and Pb (II) in comparison to Cd (II) ions during ternary metal ion system and for single metal ion system. Cd (II) adsorb more than Pb (II) and Cr (VI) on the surface of CMNPs. The value of φ and λ were in the range of 10^{-2} to 10^{4} and 10^{-12} to 10^{8}, which showed thorough coverage of CMNPs surface during biosorption with trim downed surface tension [Joos and Serrien, 1989; Ferri and Stebe, 2000]. The values of the film and pore diffusivity coefficients (Table 5.15) showed that biosorption is dependent upon pore diffusion as the values lie between 10^{-11} to 10^{-13} for Cr (VI), Pb (II), Cd (II) in single and ternary metal ion system.

5.4.0 ANN Modeling

pH, initial concentration, CMNPs dosage, contact time, agitation rate and temperature were provided as network inputs, with removal percentage being used as the target. In order to predict the output function, the feed-forward back-propagation network type, TRAINLM was taken as the training function with transfer function TANSIG that was applied in conjunction with the Levenberg-Marquardt (L-M) algorithm. After that, the network was trained until the lesser number of epochs were obtained [Kumar et al., 2019]. The experimental data was combined with the network simulation. The experimental findings were compared with prediction output function. The Mean Square Error (MSE) of the ANN model acquired in data training, testing and validation for Cr (VI), Cd (II), Pb (II) ions in single and ternary metal ion system is shown in Figures 5.22, 5.23, 5.24 and 5.25, respectively.

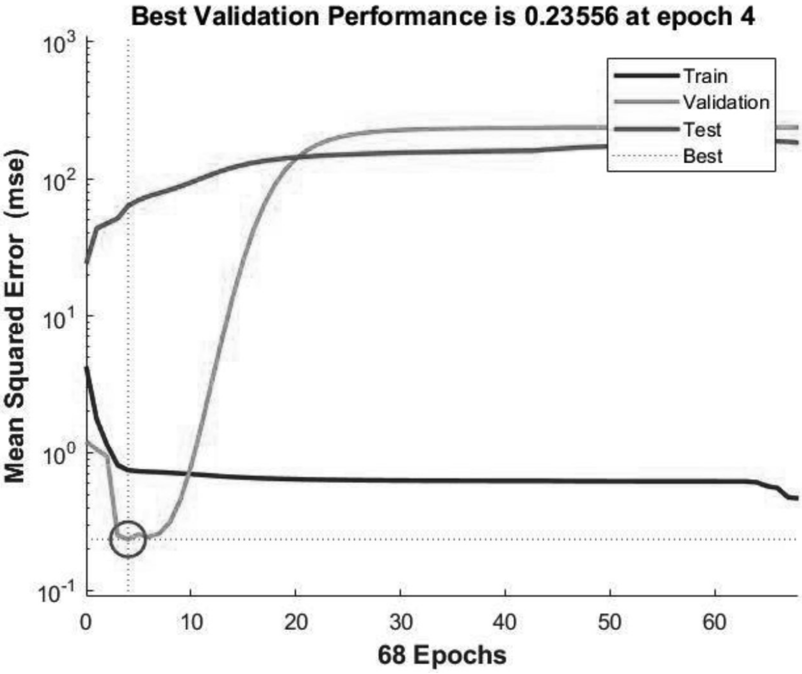

Figure 5.22 Performance between number of epochs and the MSE for Cr (VI) ions in single metal system

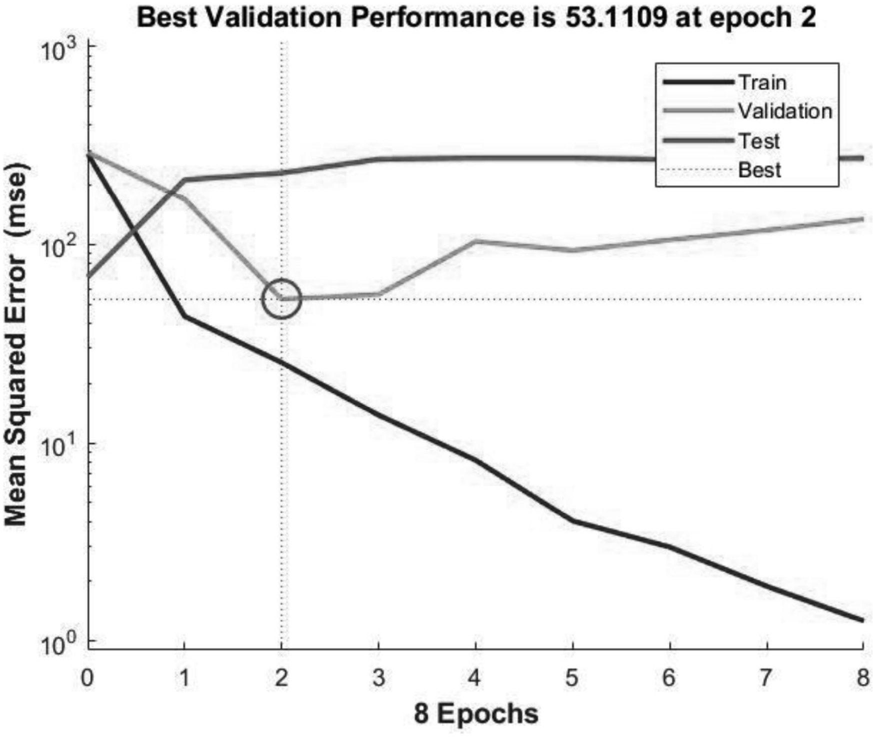

Figure 5.23 Performance between number of epochs and the MSE for Cd (II) ions in single metal ion system

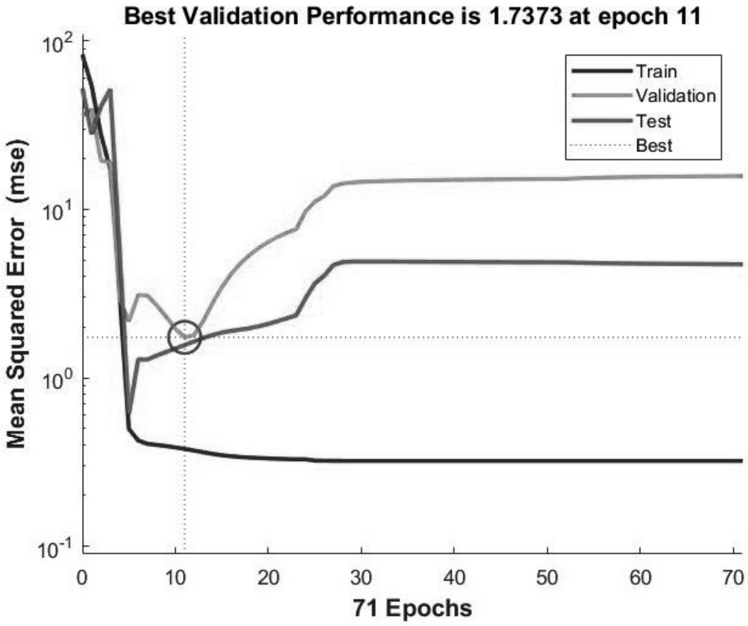

Figure 5.24 Performance between number of epochs and the MSE for lead ions in single metal ion system

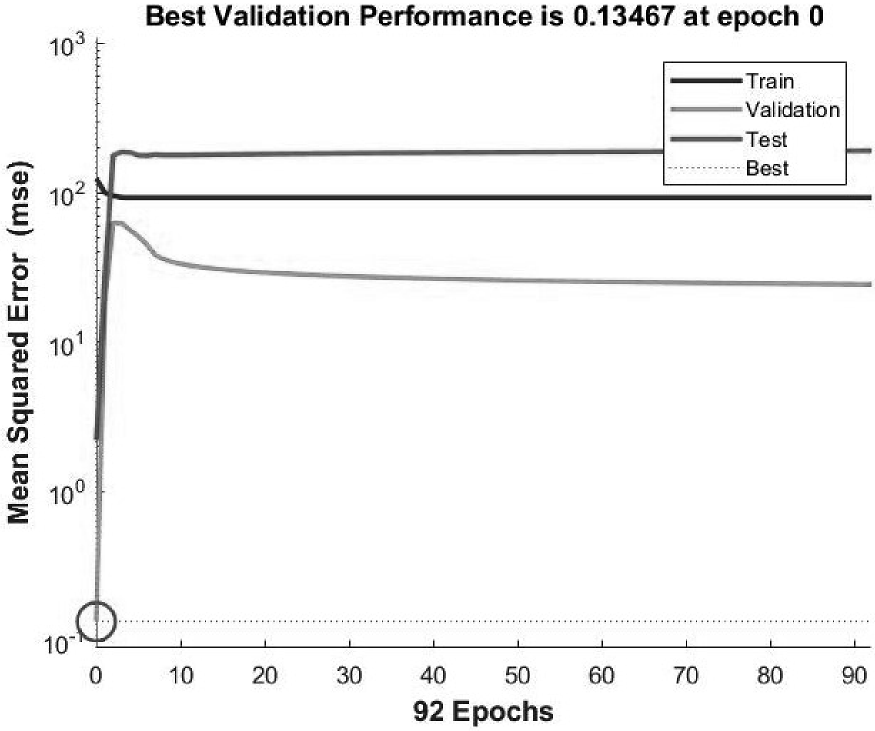

Figure 5.25 Performance between number of epochs and the MSE for ternary metal ion system

During data training, testing, and validation, the L-M algorithm reported the lowest MSE (encircled point). In the present study, the L-M algorithm was concluded appropriate for predicting the output function with the lowest MSE at epoch (4, 2 and 11 for Cr (VI), Cd (II) and Pb (II) ions in single metal ion system) and not that appropriate for MSE at epoch 11 for ternary metal ion system. It was coupled with highest validation performance in ten neurons at 0.23556, 53.1109, 1.7373 and 0.13467 for chromium, cadmium, lead ions in single metal ion system and for ternary metal ion system, respectively.

Regression between experimental and predicted values for the biosorption of Cr (VI), Cd (II), Pb (II) ion in single metal system and ternary metal ion system is shown in Figure 5.26, 5.27, 5.28 and 5.29 respectively.

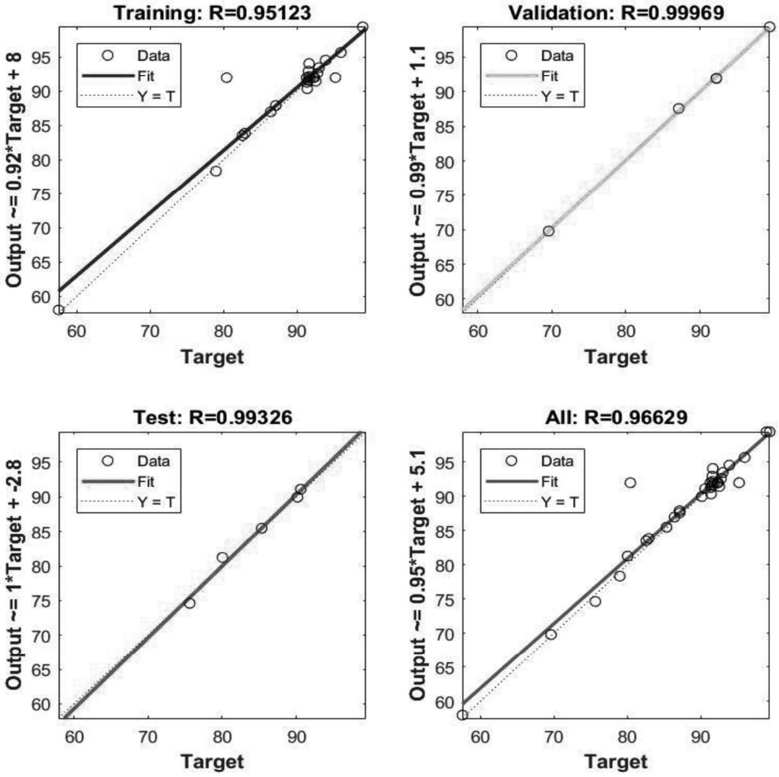

Figure 5.26 Regression plot for Cr (VI) ions in single metal ion system

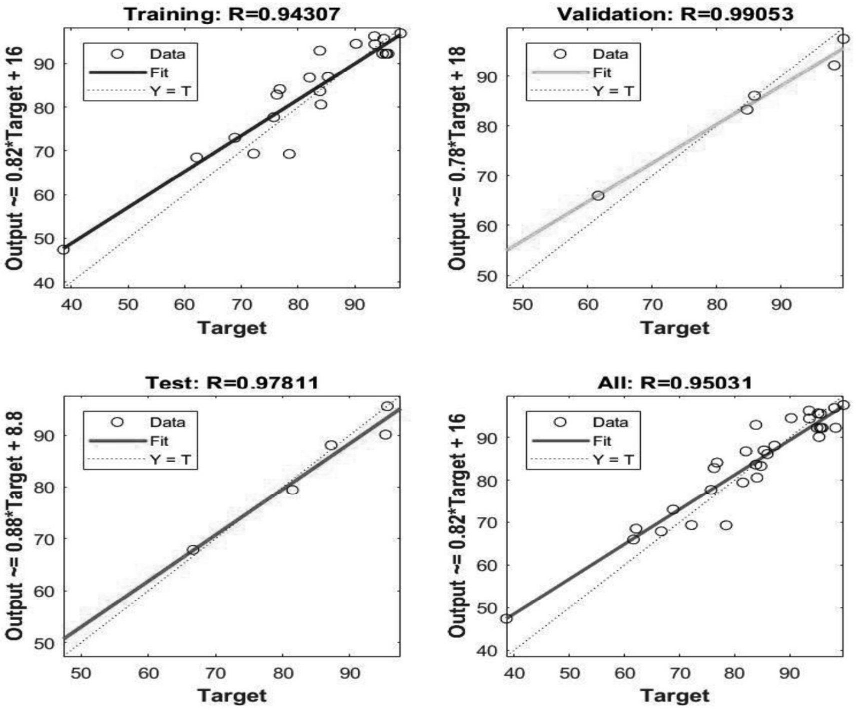

Figure 5.27 Regression plot for Cd (II) in single metal ion system

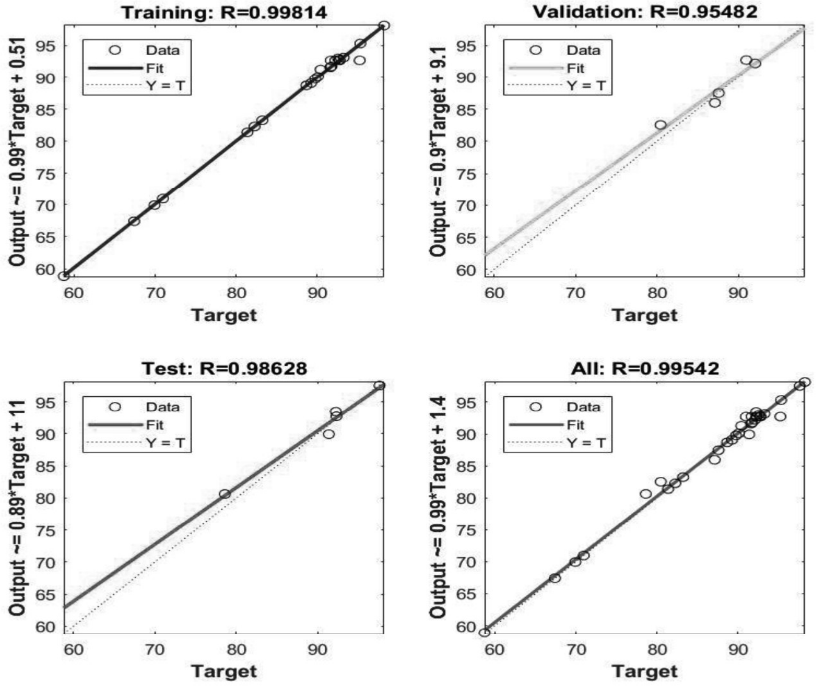

Figure 5.28 Regression plot for Pb (II) in single metal ion system

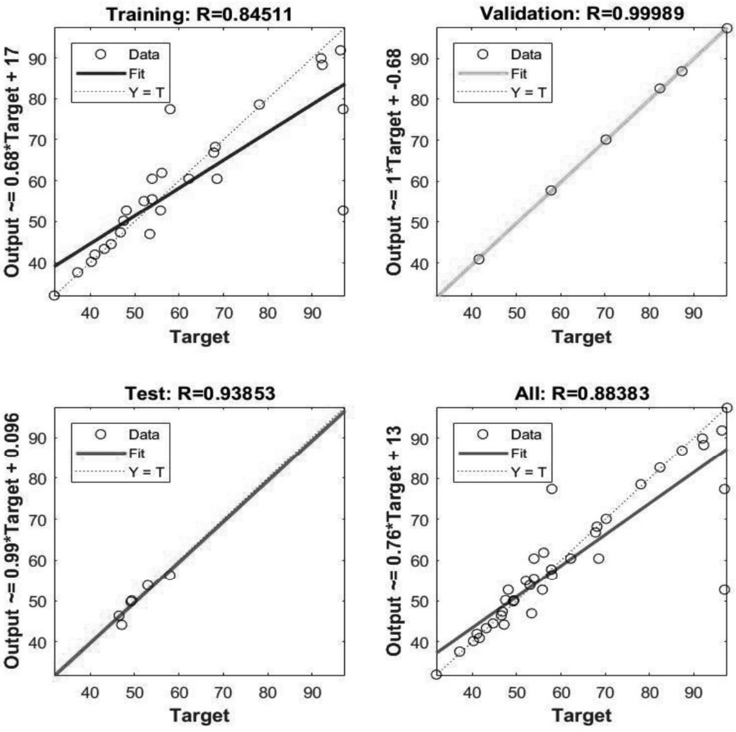

Figure 5.29 Regression plot for ternary metal ion system

The circles in the plot are experimental values and the colored lines show the predicted values derived from ANN models. Both the experimental and theoretical values seemed to be in agreement with each other showing a high regression coefficient (R^2 value in range of 0.95 - 0.99) for single (Figure 5.26, 5.27 and 5.28) and R^2 of 0.88 i.e., comparatively low in ternary metal ion system (Figure 5.29).

The correlation plot showed high regression coefficient (0.93) for Cr (VI), 0.90 for Cd (II), 0.99 for Pb (II) ions in single metal system and for ternary metal ion system R^2 was 0.92 for Cr (VI), 0.92 for Cd (II), 0.99 for Pb (II) ions between the experimental and predicted values. The results also showed a small deviation of 0.47% for Cr (VI), 0.46% for Cd (II), 0.15% for Pb (II) ions in single and for ternary metal ion system; 0.80% for Cr (VI), 1.84% for Cd (II), 0.21% for Pb (II) ion between the experimental and predicted values (Figure 5.30, 5.31, 5.32 and 5.33).

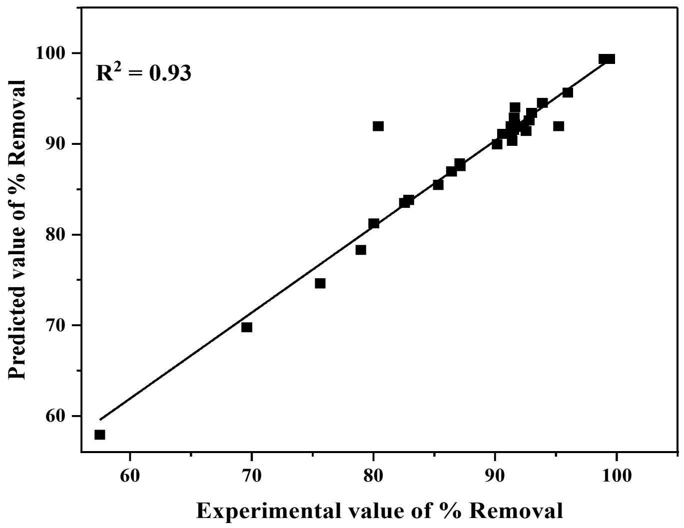

Figure 5.30 Correlation plot for the experimental and ANN predicted values for Cr (VI) ions in single metal ion system

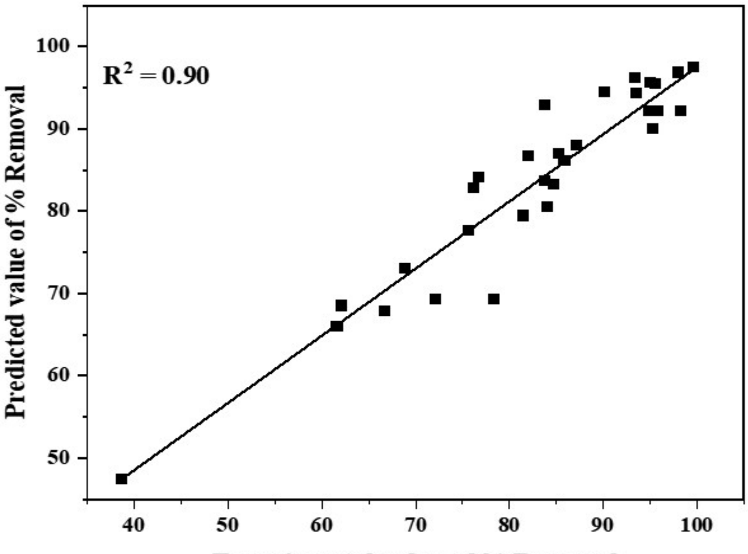

Figure 5.31 Correlation plot for the experimental and ANN predicted values for Cd (II) ions in single metal ion system

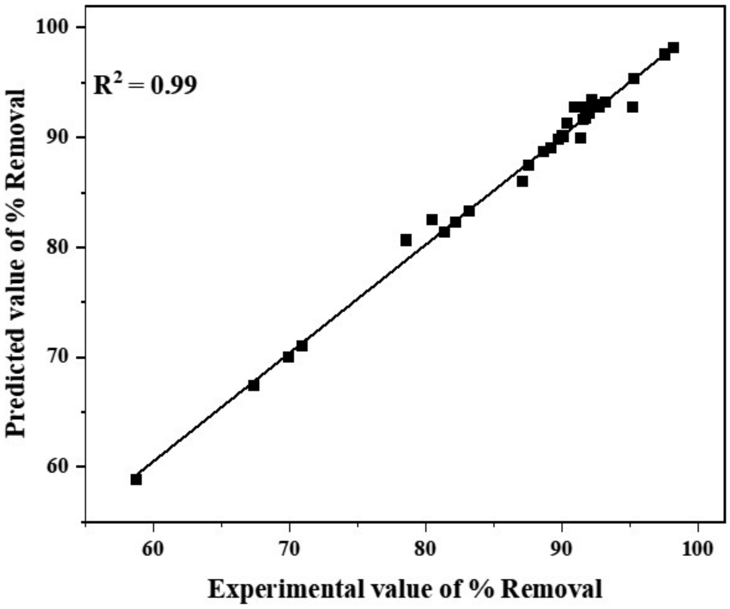

Figure 5.32 Correlation plot for the experimental and ANN predicted values for Pb (II) ions in single metal ion system

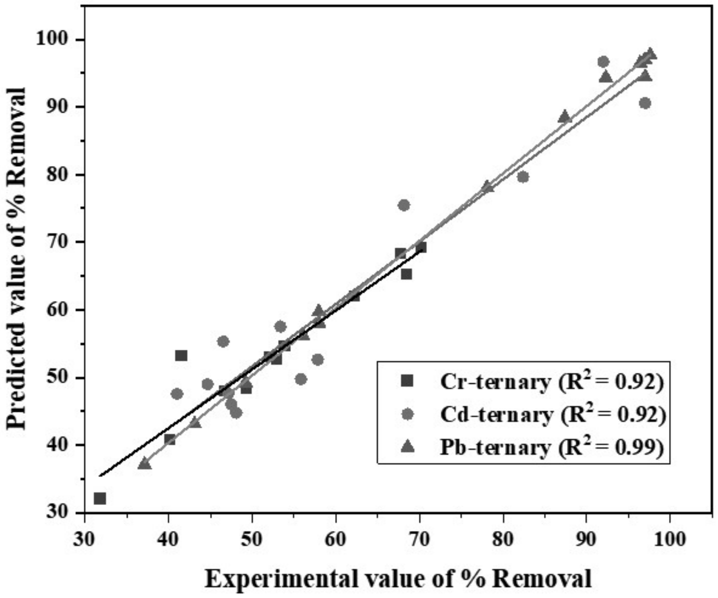

Figure 5.33 Correlation plot for the experimental and ANN predicted values for ternary metal ion system

The higher deviation of ternary metal ion system with lower regression coefficient (Figure 5.29) was observed. This further showed the suitability of L-M algorithm for both single and ternary metal ion system in the present work. According to the findings of Fan et al., 2017a, modelling and prediction of Cu (II) removal from aqueous solutions by nanocomposites using artificial neural networks. Authors revealed a strong correlation between MSE and number of epochs for the generated BP-ANN for Cu (II) removal suggested that the training was converged with the lowest MSE of 0.0002. Due to its low mean absolute error, the results predicted by this model suggested that it has better goodness of fit. Using the test sets, the average absolute error of the developed BP-ANN model was 3.64%, which revealed a good generalization of this model for the Cu (II) removal when applied to new data. Furthermore, 0.9997 of R^2 delineated better agreement between experimental and predicted values. Similarly, Fan et al., 2017b used ANN to model the removal of Cd (II) from aqueous solutions using nanoscale zero-valent iron composites and obtained R^2 value of 0.999, which showed that the predicted and experimental results were in good agreement. The average errors (%) between the experimental and predicted Cd (II) removal efficiencies were 0.0012 and 2.88, respectively, for the training and test sets. ANN model has good approximation and generalization, as evidenced by low MSE and high R^2 values for both the training and test outputs, respectively. Additionally, Narayana et al., 2021 used artificial neural networks to model the removal of Pb (II) from aqueous solutions by using iron oxide nanocomposites. The correlation coefficient between experimental data and the ANN Model was used to evaluate the model's performance. Correlation coefficients for the quadratic model were smaller than those for the present ANN model. The quadratic models have an R^2 value of 0.986, whereas the developed ANN model has an R^2 value of 0.991. The quadratic equation's average prediction error (%) was 1.502, while the ANN model's was 0.253. As a result of these findings, we concluded that the ANN model has a high degree of accuracy in predicting Pb (II) removal (%) as compared to the quadratic model estimates.

In the present work, the ANN model was demonstrated to be an excellent tool for modelling and optimizing metal ion removal with a low absolute error and a high removal efficiency, which is similar to the work presented by other researchers [Narayana et al., 2021; Fan et al., 2017a; Fan et al., 2017b].

5.5.0 Comparison of heavy metal removal capacity

The heavy metal removal efficacy of CMNPs is compared with other nanomaterials in Table 5.16.

Table 5.16 Comparison of heavy metal removal capacity of CMNPs with other nanoparticles

Nanoparticle	**Removal (%)**	**References**
Pb (II)		
Multiwall carbon nanotubes (MWCNTs)	96.03	[Kabbashi et al., 2009]
ZnO Nanoparticle	80	[Mahdavi et al., 2012]
$MnFe_2O_4$	71.10	[Eyvazi et al., 2019]
Modified activated carbon with iron	66.00	[Jiao et al., 2019]
CMNPs	94.40	[Present study]
Cd (II)		
Functionalized carbon nanospheres	52.38	[Benadji et al., 2018]
N-doped magnetic particles	16	[Li et al., 2013]

Zero-valent iron	40	[Qian et al., 2017]
graphene oxide nanocomposite	104.16	[Samuel et al., 2019]
Magnetic nanoparticle with chitosan coated	83.33	[Anush et al., 2019]
CMNPs	98.01	[Present study]
Cr (VI)		
Iron-biochar-alginate composite	86.40	[Wan et al., 2019]
Fe_3O_4/ Graphene nanocomposites	66.20	[Lv et al., 2014]
Chitosan-nanoclay composite	128.43	[Kahraman, 2017]
Montmorillonite-supported magnetite nanoparticles	15.30	[Yuan et al., 2009]
Cross linked silica gel/chitosan-g-poly nanocomposite	55.71	[Nithya et al., 2016]
CMNPs	92.19	*[Present study]*

Though these biosorption capacities have been derived in diversified experimental conditions and through different biosorption mechanisms, yet they provide significant information on nanoparticle selection for mass scale continuous industrial operations. Undoubtedly, the heavy metal removal capacity of CMNPs was greater or equivalent to most of the nanoparticles/ biomasses cited in Table 5.16.

5.6.0 Complete removal of heavy metal ions in series batch reactor system

CMNPa has high heavy metal removal capacity 92.19 % Cr (VI), 95.86 % Cd (II) and 92.77 % Pb (II) at 100 mg/L initial metal ion concentration. However, 7.81 mg/L Cr (VI), 4.14 % Cd (II) and 7.23 % Pb (II) were left in the water. This residual amount of Cr (VI), Cd (II) and Pb (II) is much higher than the permissible limit Cr (VI) (0.05 mg/L), Cd (II) (0.003 mg/L) and Pb (II) (0.01 mg/L) as demarcated by WHO, USA. Thereby, residual heavy metals were eliminated by re-treatment of first step's effluent into second batch reactor configured in series. The experiment setup of batch reactors arranged in series is shown in Figure 5.34.

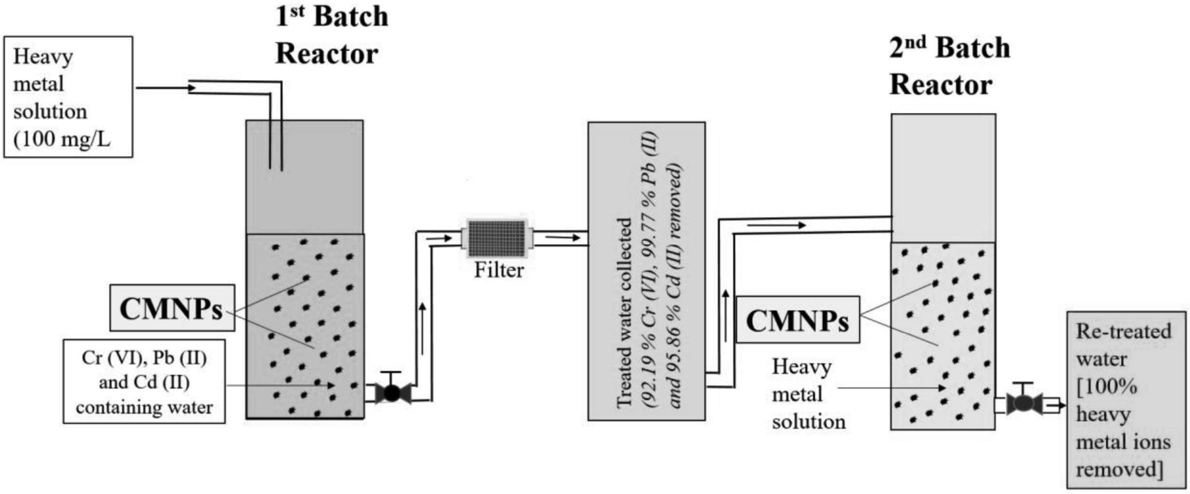

Figure 5.34 Diagrammatic demonstration of heavy metal removal in series batch reactor system

After second round treatment, 100% Cr (VI), Cd (II) and Pb (II) removal was obtained. The water treated in second round meets with permissible limit of heavy metal ion discharge in the water. CMNPs showed emerging application for removal of Cr (VI), Cd (II) and Pb (II) from water.

5.7.0 Desorption of heavy metal ions and regeneration of CMNPs

Biosorbent is considered more viable and practically advantageous when used in multiple cycles of adsorption-desorption. In this study, regeneration of CMNPs was carried out by using 0.1 N HNO_3 as eluent. The cycles of adsorption and desorption are shown in Figure 5.35, 5.36 and 5.37.

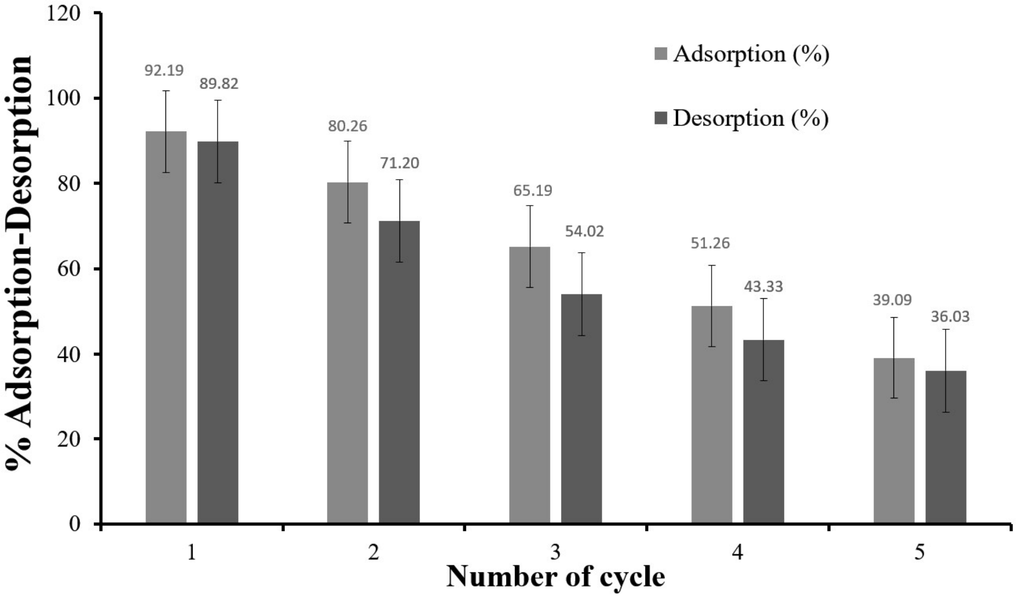

Figure 5.35 Cr (VI) adsorption - desorption on CMNPs

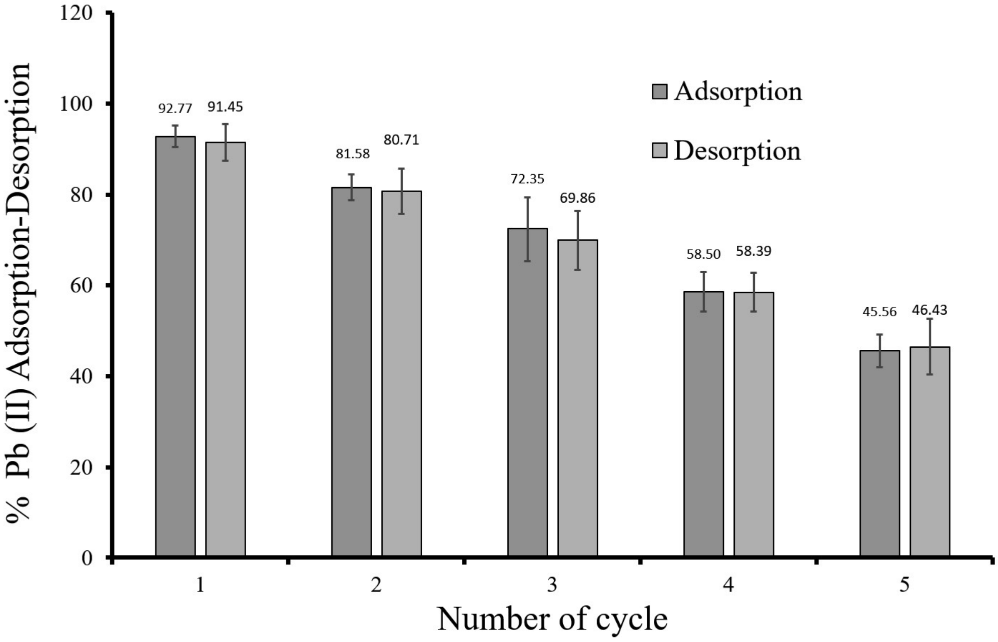

Figure 5.36 Pb (II) adsorption - desorption on CMNPs

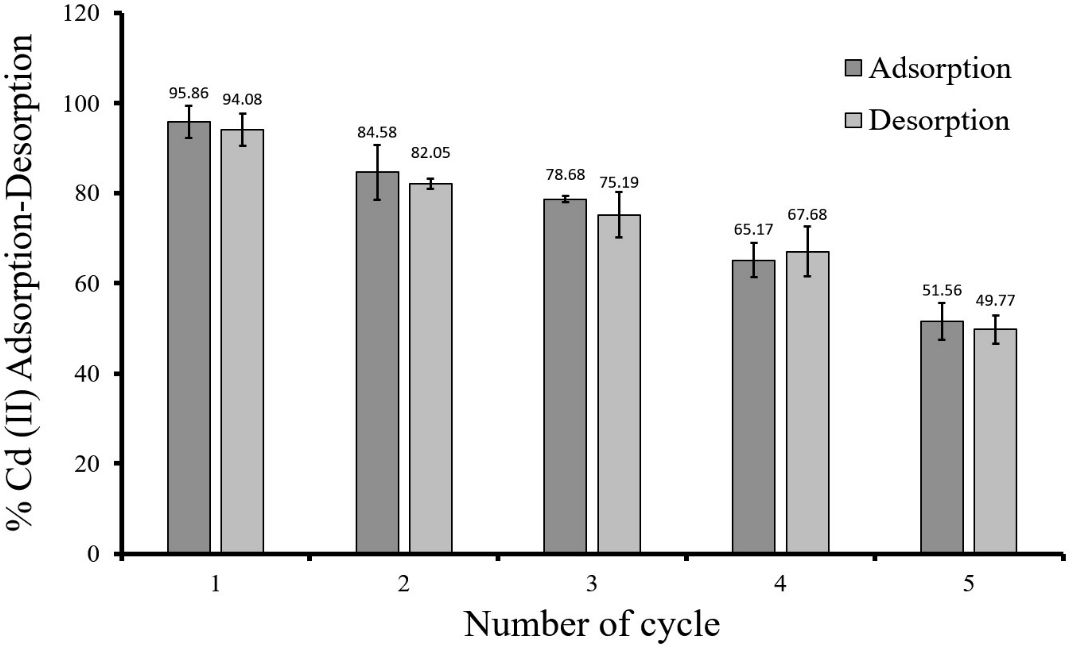

Figure 5.37 Cd (II) adsorption - desorption on CMNPs

It is apparent from Figure 5.35, 5.36 and 5.37 that % adsorption of CMNPs decreased from 92.19 to 39.09 % for Cr (VI), 92.77 to 45.56 % for Pb (II) and 95.86 to 51.56 % over five cycles of adsorption-desorption. This drop was attributed to the weight loss and deactivation of active sites of CMNPs due to repeated washing, elution and inability of eluting reagent in desorbing all adsorbed Cr (VI) ions. Though high % desorption 89.26-36.03 % for Cr (VI), 91.45 to 46.43 % for Pb (II) and 94.08 to 49.77 % was observed in complete hysteresis loop, yet it was not 100%. This was possibly due to its strong binding of heavy metal ions with CMNPs. Patra et al., 2019 reported similar observation on Cr (VI) removal by raw, acid treated and chelated-activated *Sterculia villosa* Roxb shells biomass. Authors reported that desorption-adsorption efficiency of adsorbents gradually reduced in six cycles. Bayuo et al., 2020 explored desorption efficiency of Cr (VI) and Pb (II) on groundnut husk and reported that it was reduced up to 20.0 % for Cr (VI) and 26.70 % Pb (II) after three cycles. Pandey et al., 2007 investigated Cr (VI), Pb (II) and Cu (II) adsorption-desorption on calcium alginate and reported that desorption of Cr (VI), Pb (II) and Cu (II) was decreased up to 3 %, 14 % and 15 % respectively.

The outcome of desorption study depicted the virtuous ability of regeneration and long shelf life of CMNPs over several cycles of adsorption-desorption.

5.8 Techno-economic analysis

The cost analysis is a primary approach of scaling up the heavy metal treatment opeartions [Santos-Juanes Jorda et al., 2011; Fawzy et al., 2018]. The cost estimation is helpful in the design water treatment systems [Hamdy et al., 2018]. In the present study the production cost of adsorbent (CMNPs) was estimated. The operation cost per cubic meter of water treatment was calculated through sum of chemicals/reagents and biosorbent cost. The cost/price of adsorbent preparation can be calculated as:

P_i (\$USD/g) = Raw materials cost + chemicals/regents + adsorbent preparation cost

The operation cost for treatment of heavy metal ions was calculated using following Equation

$$\text{Operation cost }((\$\text{USD/m}^3) = C_i \times P_i$$

Where, C_i (g/m^3) is the concentration of adsorbent and P_i (\$USD/g) is price of adsorbent.

In this present study, the cost of CMNPs was calculated as 0.26 \$USD/g which used for the removal of Cr (VI), Cd (II) and Pb (II) from water and 0.5 g CMNPs used for the treatment of 1 litre of water. The operation cost of CMNPs mediated heavy metal treatment was calculated and observed to be as 130 \$USD/m^3. Fawzy Et al., 2019 prepared adsorbent using Olive leaves for removal of Cr (II) and did techno-economic analysis. Authors reported similar kind of outcomes in their research.

5.9 Conclusion

The CMNPs were prepared by using curcumin extract and *Citrus limetta* peel powder. HR-SEM and TEM images of CMNPs showed rough surface, spherical shape, small size (14-25 nm) and crystallinity. DLS study represented the size distribution of CMNPs as 299.5 ± 25.32 nm. FTIR denoted presence of hydroxyl, carboxyl and amino groups. The specific surface area of CMNPs was around 76.19 m^2/g. Through EDX, XPS and elemental mapping the presence of Mn, O, C, H, and N was confirmed. The biosorption of heavy metal ions was confirmed in the EDX, elemental mapping and XPS studied. The CMNPs not only biosorbed Pb (VI), Cd (II) and Cr (VI) but also reduced Cr (VI) to Cr (III). The reduction of Cr (VI) was also confirmed through XPS. Dimensionless numbers for biosorption of Cr (VI), Cd (II), and Pb (II) on the surface of CMNPs in single and ternary metal ion system revealed that heavy metal biosorption was mix diffusion and transfer controlled. The smallest MSE i.e., 0.23556, 53.1109, 1.7373 and 0.13467, and the largest R^2 values, 0.97, 0.95, 0.99, and 0.88, were obtained with the L-M algorithm for the prediction of % removal of Cr (VI), Cd (II), and Pb (II) ions in single and ternary metal ion system, respectively. As a result, it was chosen as the best training algorithm. ANN analysis revealed that neural network modelling may be used to efficiently simulate and predict % removal.

In the single and ternary metal ion system, the Cr (VI) biosorption onto CMNPs surface indicated better goodness of fit for Freundlich isotherm (R^2 = 0.99), together with PSO kinetic model (chemisorption mode). The biosorption was endothermic, spontaneous with positive enthalpy and entropy. Cd (II) and Pb (II) biosorption in single and ternary metal ion system onto CMNPs surface indicated the better fitted in the Langmuir isotherm (R^2 = 0.99) and pseudo second order kinetic model. Thermodynamic study of Cd (II) and Pb (II) indicated the spontaneous and endothermic adsorption. The desorption study showed that CMNPs can be reused for several cycles with a long shelf life. Comparison among biosorption capacities of various nanoparticles proved that CMNPs are effective and potent heavy metal ions scavenger. In this study, 92.19 % Cr (VI), 92.77 % Pb (II) and 95.86 % Cd (II) was removed by CMNPs from water. The heavy metal removal pattern was reported in this study was Cd (II) > Pb (II) > Cr (VI). The complete removal of heavy metal ions from water was achieved by using batch reactors in series, which removed heavy metal concentration below the permissible limit of discharge as demarcated by WHO, USA and CPCB, India.